EMC Measurements in the Time-Domain

Peter Russer
Institute for Nanoelectronics, Technische Universität München, Arcisstrasse 21, Munich, Germany
Email: russer@tum.de

Abstract

In this tutorial presentation, broad-band time-domain electromagnetic interference (EMI) measurement techniques are discussed. Time-domain EMI measurement systems are based on broad-band analog-to-digital conversion and subsequent real-time digital processing of the EMI measurement signals. This allows us to reduce the measurement times by several orders of magnitude. Modern time-domain EMI measurement systems for frequency bands up to 18 GHz and their principles of operation are presented. Like conventional EMI receivers, time-domain EMI measurement systems facilitate the measurement of average-, rms, peak-, and quasi-peak values of the EMI. Additionally, time-domain electromagnetic interference measurement systems allow measuring phase-spectra, short-time spectra and to performing statistical analysis of the measured signals.

1 Introduction

The development of electronic circuits and systems towards enhanced functionality and performance, increased complexity and integration density, and higher bandwidth not only increases the requirements concerning technology and design methods but also on high frequency and electromagnetic compatibility measurement techniques. Due to the high bandwidth and their low power levels, modern electronic systems are highly sensitive to electronic disturbances. *Electromagnetic Compatibility* (EMC) is the topical area dealing with the accidental generation, propagation, and reception of electromagnetic energy especially in reference to the objectionable effects, summarized under *Electromagnetic Interference* (EMI) [1–4]. Electromagnetic Compatibility denotes a situation where electrical and electronic systems are not mutually interfering by electric, magnetic or electromagnetic interference. The guideline 2004/108/EG of the European Community [5] defines Electromagnetic Compatibility as "the ability of equipment to function satisfactorily in its electromagnetic environment without introducing intolerable electromagnetic disturbances to other equipment in that environment". That document also defines "electromagnetic disturbance" as "any electromagnetic phenomenon which may degrade the performance of equipment" and states: "An electromagnetic disturbance may be electromagnetic noise, an unwanted signal or a change in the propagation medium itself."

Modern electric and electronic systems have to be designed and realized such that the escape of unwanted electromagnetic energy into the environment is minimized. This requires the characterization of the conducted and radiated electromagnetic interference of electric and electronic systems in the complete frequency range from low frequencies up to the microwave region.

Broad-band measurement systems for the measurement of electromagnetic interference are important tools required in development of electric and electronic products and for the test of their electromagnetic compliance. Traditionally, measurements of electromagnetic interference are performed using EMI receivers operating by the superheterodyne principle. For the characterization of a device under test, according to the international EMC standards, the measurements must be performed at thousands of frequency points sequentially. Due to a dwell time of several seconds at every frequency bin the total measurement time may be several hour [1–3, 6, 7].

Time-domain EMI measurement systems sample the broad-band EMI signal with GHz sampling rates and compute the EMI spectrum by digital signal processing, e.g. by the fast Fourier transform (FFT). This yields a considerable reduction of the measurement time by up to five orders of magnitude. Time-domain measurement of EMI has been suggested for the first time by E.L. Bronaugh [8, 9]. Further early work on time-domain EMI measurement was published in [10, 11]. M. Parvis et al have realized a time-

978-1-4244-6051-9/11/$26.00

domain EMI precompliance test set for conducted emission measurements based on a sampling oscilloscope with subsequent discrete Fourier transform (DFT) signal processing [12]. A time-domain Fast Emission Measurement system (FEMIT) using DFT for spectral estimation has been presented by C. Keller [13–15].

Florian Krug developed a time domain electromagnetic interference measurement system that uses ultra high-speed analog-to-digital converters and real-time digital signal processing systems to enable ultra fast tests and measurements for electromagnetic compliance [16–22]. In 2004, Stephan Braun realized a first time-domain EMI measurement system for the frequency range from 30 MHz to 1 GHz in [23–28]. The system performs the calculation of the spectrum by the fast Fourier transform (FFT) and a simultaneous evaluation of the spectrum in the peak, average, and root-mean-square detector mode. In [29–36], the suitability for full compliance measurements has been demonstrated. With the time-domain EMI measurement system described in [37, 38], a reduction of the measurement time by a factor of 8000 was achieved. Applying three parallel analog-to-digital converters a multi-resolution system was realized that fulfills the international EMC standards CISPR 16-1-1 [39]. Ambient cancellation techniques in time-domain for full compliance EMI measurements are investigated in [40, 41]. In this system two channels are fed from two broad-band antennas, where the first antenna is receiving predominantly the EMI radiated from the device under test and a second antenna receives predominantly the ambient noise. These techniques allow fast measurements of electromagnetic interference in the time-domain at open area test sites.

A joint working group between CISPR A/1 (EMC Instrumentation Specifications) [42], CISPR A/2 (EMC Measurement Methods, Statistical Techniques and Uncertainty) [43], and CISPR D/2 (Protection of On-Board Receivers) has been formed in order to perform the expansion of the international EMC standards CISPR 16-1 and CISPR 16-2 to time-domain EMI measurement systems that use the FFT for the calculation of the spectrum. The newest CISPR 16-1-1 Ed. 3 Am. 1 [44] adds specifications like gapless acquisition for time-domain EMI measurement systems.

In Section 2, the meaning and significance of electromagnetic interference is discussed briefly. Section 3 summarizes some important terms and definitions, and in Section 4, fundamentals and standards of EMI measurements are treated. The conventional EMI measurement method with heterodyne receiver is discussed in Section 5. This method has set the standards for EMI measurement which also have to be considered in time-domain measurement. Section 6 introduces into the discrete time signal processing methods upon which discrete-time EMI measurement systems are based. In Subsection 6.1, the fundamentals of signal windowing sampling and signal representation by short-time spectra are discussed. Subsection 6.2 gives an account on the power spectra of random signals. Digital signal processing is treated in Section 7, where in Subsection 7.1 digital Fourier transformation and in Subsection 7.2 the periodogram are introduced. In Subsection 7.3 the influence on the signal quantization on the signal–to–noise relation is discussed. In Section 8, modern commercial time-domain EMI measurement systems are described. A system with one analog-to-digital converter (ADC) is discussed in Subsection 8.1. The quantization noise limitations of one-ADC-systems were overcome with systems with three ADCs which allow full compliance measurements up to 1 GHZ after CISPR standard [42]. Systems applicable to frequencies up to 18 GHz are described in Subsection 8.3. A system applying ambient noise cancellation techniques as described in Section 9 can be used outside anechoic chambers in noisy environments.

2 What is Electromagnetic Interference?

Electromagnetic interference (EMI) deals with the generation, transmission and reception of unintended electromagnetic signals. A simple description of the electromagnetic interference phenomena can be given by an interference coupling model subdividing the EMI structure under consideration into *source*, *coupling path*, and *victim*. We distinguish between *radiated emissions* and *conducted emissions* along wiring and transmission lines. The coupling path can be *conductive*, *inductive*, *capacitive*, and/or *radiative* as shown schematically in Fig. 1. Inductive and capacitive coupling are near-field effects and only play a role in the near vicinity of the source. EMI can occur in a wide spectral range from low frequencies up into the

millimeterwave range and beyond. The frequency range in which electromagnetic interference has to be observed depends on the frequency range in which victims are sensitive.

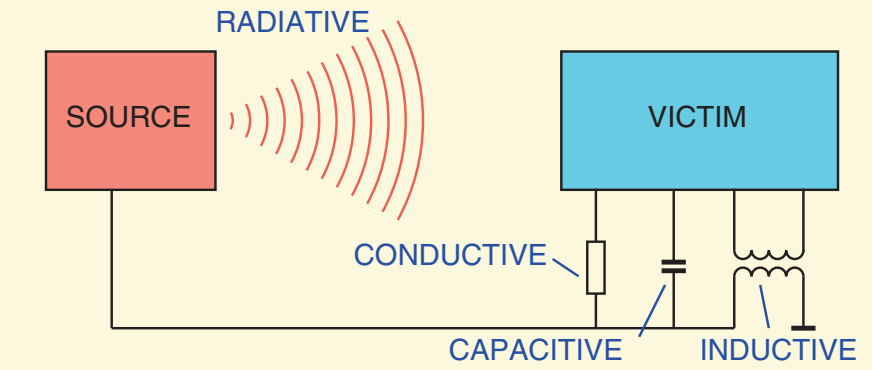

Figure 1: EMI coupling models.

Electromagnetic interference can be continuous or transient and impulsive, respectively. Continuous interference is emitted from power amplifiers, transmitters, receivers, and industrial and medical RF systems. Broad-band noise signals belong to continuous EMI. Transient or impulsive electromagnetic interference, also called electromagnetic pulse (EMP) or transient disturbance, occur when electric currents are switched, especially in the case of inductive load and in connection with electric discharges. EMPs are radiated from electric machines.

Several international organizations work on the international harmonization of standards and regulations. The International Electrotechnical Commission (IEC) is the world's leading organization preparing and publishing standards for electrical and electronic technologies [4, 45]. Within the IEC the following committees are interested in the reduction of electromagnetic interference and concerned with EMC issues:

- The Comité International Spécial des Perturbations Radioeléctriques - CISPR (International Special Committee on Radio Interference), founded in 1934, develops standards concerning EMI and immunity with respect to EMI and and EMC measurement [46]. More than thirty CISPR standards have been published so far.
- The IEC Technical Committee 77 (TC77) prepares standards and technical reports on EMC, considering general applications and use by product committees.
- The IEC Advisory Committee on Electromagnetic Compatibility (ACEC) advises the IEC Standards Management Board and coordinates IEC activities on EMC issues in order to ensure consistency in IEC standards.

The International Organization for Standardization (ISO), developing international standards on a variety of subjects, including EMC in the context of special industrial product categories [47]. In Europe the Comité Européen de Normalisation (CEN) [47], the Comité Européen de Normalisation Electrotechniques (CENELEC) [48], and the European Telecommunications Standards Institute (ETSI) [49], in the USA the Federal Communications Commission (FCC) [50], in Britain the British Standards Institution (BSI), and in Germany the Verband der Elektrotechnik, Elektronik und Informationstechnik (VDE) are also concerned with the definition of EMC standards.

Electric, electronic, and other industrial products have to be designed, manufactured and installed in a way such that conducted as well as radiated electromagnetic interference is minimized. Compliance with national and international standards is regulated by laws enacted from the national governments. European

law is harmonized concerning EMC and the manufacturers of electronic devices are requested to perform EMC test in order to comply with the compulsory CE-labeling of their products. The directive 2004/108/EC [49] has the objective to regulate the compatibility of equipment regarding EMC. According to this directive equipment "has to comply with EMC requirements when it is placed on the market and/or taken into service" and "the application of good engineering practice is required for fixed installations, with the possibility for the competent authorities of member states to impose measures if non-compliance is established". The directive 2004/108/EC limits the emission of equipment so that it does not disturb other equipment. Furthermore, this directive also regulates the immunity such that equipment is not disturbed by other equipment, compliant with the regulations.

3 Terms and Definitions

In the following we present some terms and definitions which are meaningful in the context of EMI measurements [42]:

- The *bandwidth* B_n is the frequency interval between two points of an attenuation of n dB. The CISPR 16–1–1 definitions usually refer to the 6 dB bandwidth B_6.
- An *impulse area*, also called *impulse strength* IS, is defined for impulse voltage signals $V(t)$ as

$$IS = \int_{-\infty}^{\infty} V(t)dt. \tag{1}$$

  The impulse area is expressed either in μVs or dB(μVs). The *spectral density*, expressed in μV/MHz or dB(μV/MHz) is related to the impulse area. For rectangular impulses with pulse width T and pulse rates $f \ll 1/T$ the relationship is given by $D\,(\mu\text{V/MHz}) = \sqrt{2} \times 10^6\ IS\,(\mu\text{Vs})$.
- The *impulse bandwidth* B_{imp} of a receiver is defined as

$$B_{imp} = \frac{A(t)_{max}}{2\,G_0\,IS}, \tag{2}$$

  where $A(t)_{max}$ is the peak value of the envelope $A(t)$ of the signal at the intermediate frequency (IF) output of the EMI receiver. IS refers to the input signal $V(t)$ of the receiver and G_0 is the gain from receiver input to IF output. The impulse bandwidth B_{imp} is related to the 3 dB bandwidth B_3 and the 6 dB bandwidth B_6 by

$$B_{imp} = 1.05B_3 = 1.31B_6. \tag{3}$$

4 Fundamentals and Standards of EMI Measurements

For the measurement of the EMI spectrum over a broad frequency band and with high spectral resolution spectral analyzers or EMI receivers are used [42]. We distinguish between conducted and radiated emissions. CISPR 16-1-1 defines a limit for the conducted emission, which at any connecting pin of external lines should not exceed a specified limit. For conducted emission measurements, the device or system under test is connected to the EMI receiver via cable. For radiated emissions the device or system under test is placed either in a free range test site, in a transverse electromagnetic cell (TEM-cell), a reverberation chamber, or into an anechoic chamber. CISPR 16-1-1 specifies the limits of the radio disturbance field strength emitted by the EMI receiver in the frequency range from 9 kHz to 18 GHz [42].

Figure 2 shows an EMI measurement test setup in an anechoic chamber. The inner side of the metallic screening walls of the chamber usually are first covered with ferrite plates and upon these with high-frequency absorbing material. The device or system under test is positioned on a rotation table, so that its angular

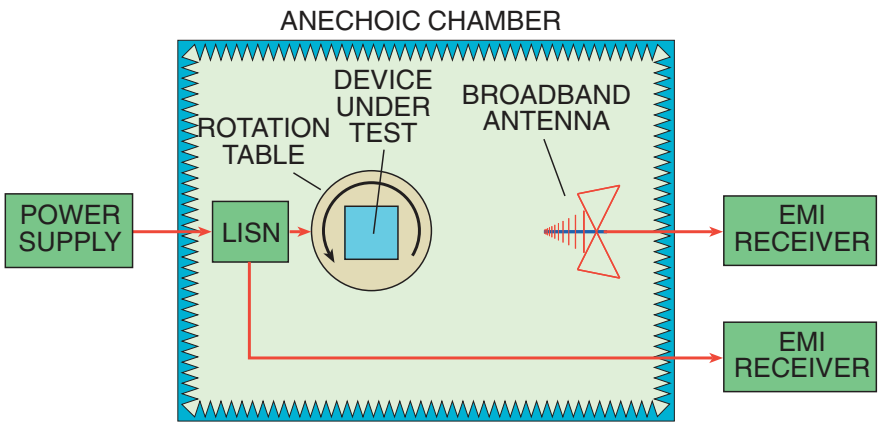

Figure 2: Electromagnetic interference measurement setup.

position can be controlled. The conducted EMI is measured via a line impedance stabilization network (LISN). The LISN is a low-pass filter network that provides a known impedance of the power line for the connected device under test, blocks electromagnetic interference coming from the power line, and transfers the electromagnetic interference from the device under test to the EMI receiver [1, p. 450]. The conducted disturbance voltage is usually measured in the frequency range from 9 kHz to 30 MHz. The radiated EMI is received by a broad-band antenna and fed into an EMI receiver. The radiated EMI is usually measured from 30 MHz up into the GHz range.

The international standard for radio disturbance and immunity measuring apparatus methods are defined in the document CISPR 16-1-1 [42]. Part 1-1 of this document deals with the radio disturbance and immunity measuring apparatus for the measurement of radio disturbance voltages, currents, and fields in the frequency range from 9 kHz t 18 GHz.

The American National Standard for electromagnetic noise and field strength instrumentation provides a summary of the characteristics for quasi-peak-, peak-, average-, and rms-average EMI measuring instrumentation in the frequency range from 10 Hz to 18 GHz and refers to CISPR 16-1-1 [42, 51]. US national deviations to CISPR 16-1-1 in the ANSI C63.2-2009 standard exhibit a starting frequency of 10 Hz with an upper frequency of 40 GHz with field strength requirements of 0.01 μV for 10 Hz to 20 kHz, 0.5 μV for 9 kHz to 1 GHz, and 2.2 μV to 3.0 μV for 1 GHz to 40 GHz [51].

5 EMI Measurements in Frequency Domain

Since the mid of the thirties of the past century the traditional method to carry out electromagnetic interference measurements is based on the use of EMI receivers operating in the frequency domain. [1–3, 7]. The required frequency resolution is achieved by narrow-band filtering of the interference signal. Measurements according to the international EMC standards [43] have to be performed sequentially at several thousand frequency bin positions. Due to a dwell time of several seconds at every frequency point the complete characterization of a device under test may take several hours. These EMI receivers perform a bandpass filtering of the EMI signal and a downconversion to an intermediate frequency. The IF-signal is demodulated and evaluated by the various detector modes, e.g. the average, rms, peak, and quasi-peak detector modes [42].

Figure 4 shows the block diagram of a conventional EMI receiver. The EMI signal is filtered in the RF preselection bandpass filter BPF1, amplified in the low-noise amplifiers LNA yielding the signal with spectrum S_{IN} fed into the mixer M, where the signal from the local oscillator LO with frequency f_{LO} is superimposed. The intermediate frequency output signal of the mixer M is filtered in a bandpass filter

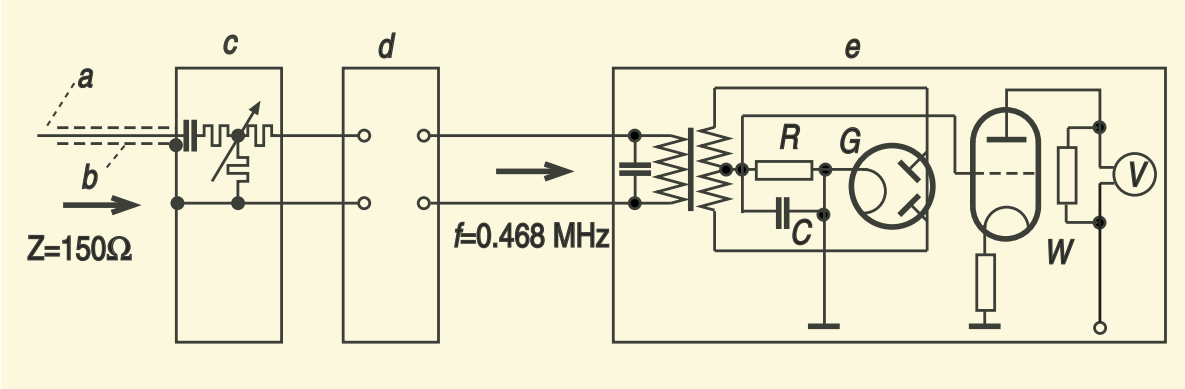

Figure 3: Frequency domain measurement system after Hagenhaus [7].

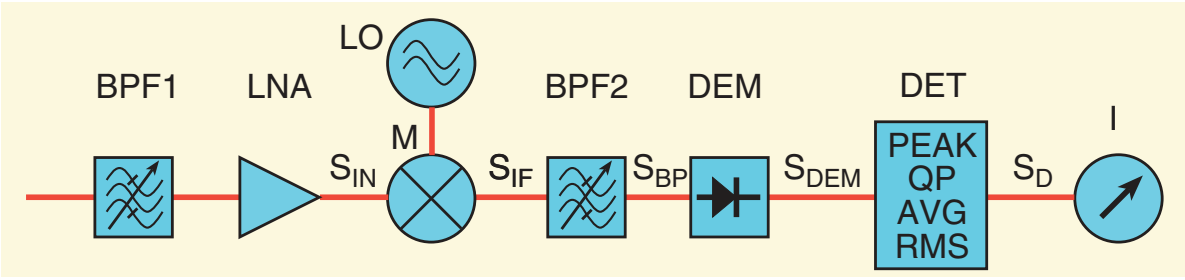

Figure 4: Block diagram of an EMI receiver.

BPF2. The bandpass filter determines the bandwidth and the linear signal transfer characteristics of the EMI receiver. In the demodulator, the IF signal $S_{IF}(f)$ is rectified and, by an integrator or low-pass filter, limited to the base band, which has half the width of the IF band. The detector DET further processes the demodulator output signal $S_{DEM}(f)$. This value is displayed by critically damped mechanical indicating instrument I.

Let us consider the signal processing of the analogue frequency-domain EMI receiver. The spectrum of the mixer output signal is

$$S_{IF}(f) = S_{IN}(f - f_{LO}). \tag{4}$$

The output signal of the mixer is filtered in the bandpass filter BPF2 with the transfer function $H_{BP}(f)$ yielding

$$S_{BP}(f) = H_{BP}(f) S_{IF}(f). \tag{5}$$

The bandpass filter BPF2 determines the bandwidth of the EMI receiver. The bandwidth requirements according to CISPR 16-1-1 [42] depend on the frequency band. The bandwidth shall be within the values given in Table 1.

The time-domain signal $s_{BP}(t)$ corresponding to the spectrum $S_{BP}(f)$ is given by

$$s_{BP}(t) \circ\!\!-\!\!\bullet\, S_{BP}(f), \tag{6}$$

where the symbol $\circ\!\!-\!\!\bullet$ denotes the Fourier transform.

In the case of a *linear mean value demodulator*, the absolute value of $s_{BE}(t)$ is formed and averaged over a time interval from $(t - \Delta t)$ to t. In this case the output signal $s^{ml}_{DEM}(t)$ of the detector D is given by

$$s^{ml}_{DEM}(t) = \int_{t-\Delta t}^{t} |s_{BP}(t_1)|\, dt_1. \tag{7}$$

Table 1: Bandwidth Requirements according to CISPR 16–1–1 [42, p. 26, p. 31].

Band	Frequency Range	6 dB Bandwidth B_6
A	9 kHz – 150 kHz	200 Hz
B	150 kHz – 30 MHz	9 kHz
C and D	30 MHz – 1 GHz	120 kHz
E	1 GHz – 18 GHz	1 MHz

In the *square law mean value demodulator* the signal is squared and averaged over the time interval from $(t - \Delta t)$ to t, yielding the detector output signal

$$s_{DEM}^{sl}(t) = \int_{t-\Delta t}^{t} s_{BP}(t_1)^2 dt_1. \tag{8}$$

In the case of analog signal processing the mean value usually is performed by analog integrators realized with RC circuits. If the pulse response function of the analog integrator is given by $h_{int}(t)$, the output signals $s_D^{ml}(t)$ of the linear demodulator and $s_D^{sl}(t)$ for the square law demodulator are given by

$$s_D^{ml}(t) = \int_{-\infty}^{t} |s_{BP}(t_1) h_{int}(t - t_1)| \, dt_1, \tag{9a}$$

$$s_D^{sl}(t) = \int_{-\infty}^{t} s_{BP}(t_1)^2 h_{int}(t - t_1) dt_1. \tag{9b}$$

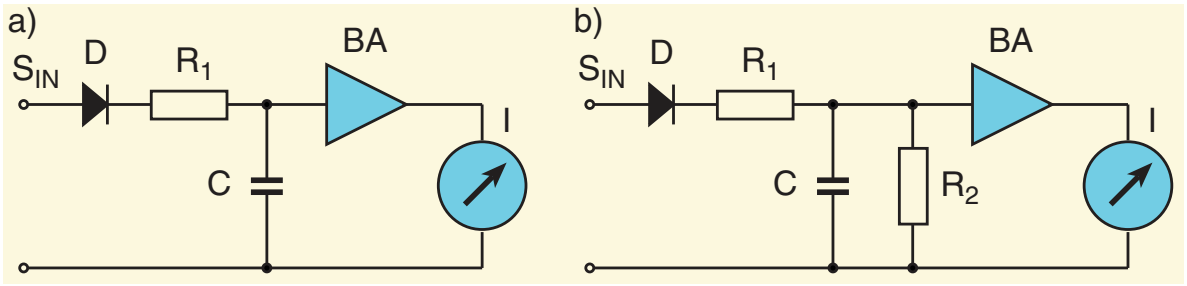

Figure 5: Analog circuit of (a) a peak detector and (b) a quasi-peak detector.

The EMI measurement receivers covered in CISPR 16-1-1 and ANSI C63.2 documents [42, 51] include the following detector modes:

- The *peak detector* has a peak-value holding capability. Figure 5 (a) shows the analog maximum-hold circuit realization of a peak detector. The RC circuit formed by R_1 and C exhibits a time constant

$$\tau_c = \frac{1}{R_1 C}. \tag{10}$$

  The input signal $s_{IN}(t)$ charges the capacitor C with the time constant τ_c. The charge time constant is the time that passes until the detector output signal reaches 63 % of its final value after, with a step-like transition, a continuous wave RF signal is applied to the EMI receiver input. Since the buffer amplifier BA has an input impedance by several orders of magnitude higher than R_1, the capacitor C holds the peak value of the voltage for a long time indicating the peak value measured over a long time interval of the interference signal. Furthermore, we have to consider a time constant τ_m of the critically damped mechanical indicating instrument I. In order to obtain a meter reading deviation within 10 % of the true value at a pulse repetition rate of 1 Hz, the ratio charge time constant τ_c to discharge time constant should be equal or greater than the values specified in Table 2 [42, p. 23].

Table 2: Bandwidth Requirements according to CISPR 16-1-1 [42, p. 23].

Band	Frequency Range	Minimum τ_d/τ_c
A	9 kHz – 150 kHz	1.89×10^4
B	150 kHz – 30 MHz	1.25×10^6
C and D	30 MHz – 1 GHz	1.67×10^7
E	1 GHz – 18 GHz	1.34×10^8

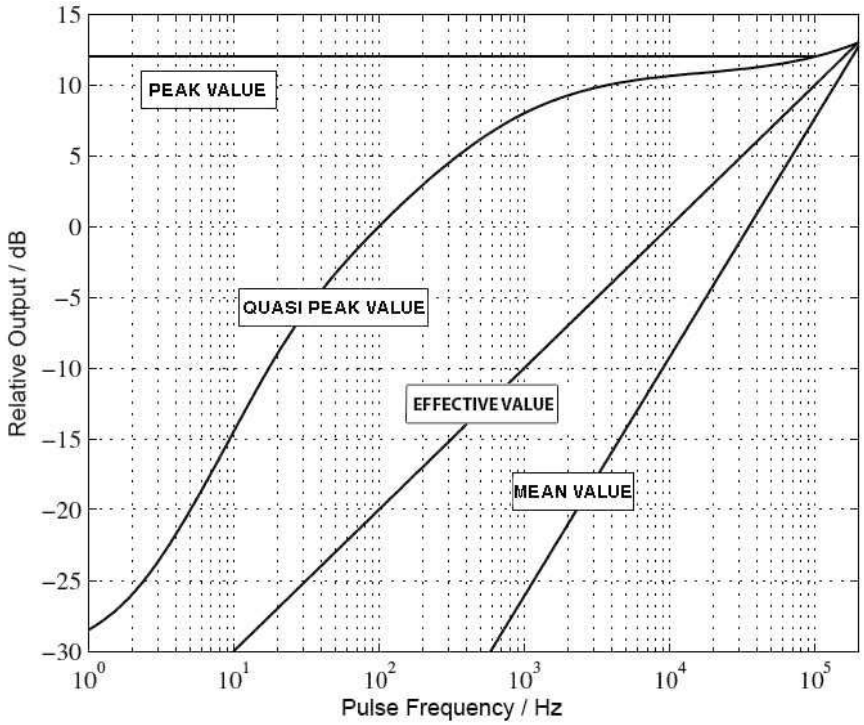

Figure 6: Pulse response curves of EMI receivers [52].

Figure 6 shows the pulse response curves of an EMI receiver in the various detector modes [52]. In the peak detector mode, the peak value of impulsive perturbations can be measured even if the EMI pulse repetition rate is very low.

- The *quasi-peak detector* prescribed in CISPR and FCC measurement procedures is similar to an *RC* maximum-hold circuit, but exhibits a certain time constant τ_2 for discharge. The analog circuit of a quasi-peak detector is shown in Fig. 5 (b). The quasi-peak detector is charged with the time constant τ_c and discharged with the time constant τ_d given by

$$\tau_d = \frac{1}{R_2 C}. \tag{11}$$

The characteristics of quasi-peak receivers according to CISPR 16-1-1 are summarized in Table 3.

- The *average detector* forms the mean value of the demodulated IF signal $s_{DEM}(t, f)$ over a time interval T_D, where f is the frequency to which the EMI receiver is tuned. In general, average detectors are used for narrowband interference signals and not for impulsive disturbances. The mean value $s_D^{avg}(t, f)$ over T_D is given by

$$s_D^{avg}(t, f) = \frac{1}{T_D} \int_{t-T_D}^{t} s_{DEM}(t_1, f) dt_1. \tag{12}$$

Table 3: Characteristics of Quasi-Peak Receivers according to CISPR 16-1-1 [42, p. 10].

Characteristics	Frequency Band		
	Band A 9 kHz – 150 kHz	Band B 150 kHz – 30 MHz	Band C 30 MHz – 1 GHz
6 dB Bandwidth B_6	200 Hz	9 kHz	120 kHz
τ_c	45 ms	1 ms	1 ms
τ_d	500 ms	160 ms	550 ms
τ_m	160 ms	160 ms	100 ms
Overload Factor of Circuits Preceding the Detector	24 dB	30 dB	43.5 dB
Overload Factor of the DC Amplifier and Indicating Instrument	6 dB	12 dB	6 dB

The noise floor of the average detector is 12 dB lower than that of the peak detector [53]. This allows to detect narrow-band interferers which otherwise would be buried in noise [54].

- The *rms–average detector* forms the effective value of the demodulated IF signal $s_{DEM}(t, f)$, averaged over a time interval T_D. The rms value $s_D^{avg}(t, f)$ over T_D is given by

$$s_D^{rms}(t, f) = \sqrt{\frac{1}{T_D} \int_{t-T_D}^{t} s_{DEM}^2(t_1, f) dt_1}. \tag{13}$$

The noise floor of the rms–average detector is by 1.2 dB higher than that of the average detector [55].

6 Discrete–Time Signal Processing

Time-domain EMI measurement systems are based on a complex discrete-time signal processing. The mathematical framework for designing spectrum analysis systems is given by the theory of Fourier analysis. Investigating EMI we have to deal with time continuous signals of potentially infinite extension in time. However, in practice we can extend our measurements only over finite time intervals and for digital signal processing we are restricted to measure sequences of time-discrete signal samples. Furthermore, either due to the physical nature of the electromagnetic interference under consideration or due to our lack of knowledge, we have to consider the signals to be measured as stochastic ones. The design of a time-domain EMI measurement system has to be performed on these given factors.

The discrete Fourier transformation, which is the basis of the numerical computation of amplitude spectra, has been described for the first time by Carl Friedrich Gauss in his treatise written in 1805 "*Theoria interpolationis methodo nova tractata*" [56]. Gauss has not considered this work worth being published and so it has not been published before 1866, after he passed away. Time-domain EMI measurement systems measure the base-band signal in time domain and compute the signal spectrum by Fourier analysis from this measured time-signal. In 1822, Jean Baptiste Fourier suggested that a periodic temperature distribution can be described by a linear combination of sine and cosine functions [57]. The proof has been given in 1829 by Peter Gustav Lejeune Dirichlet [58].

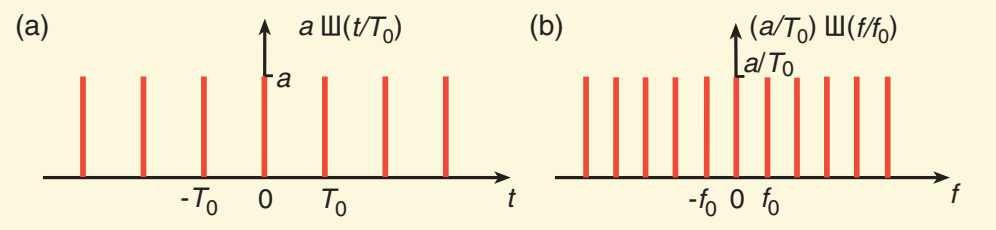

Figure 7: (a) Time function $s_A(t)$, (b) Spectrum $S_A(f)$ of a periodic Dirac pulse sequence.

6.1 Sampling and Analog–to–Digital Conversion

Time-domain EMI measurement systems are based on digital signal processing. In an analog-to-digital converter the EMI signal first is sampled with a sampling frequency f_0. The sampling period Δt is given by

$$\Delta t = \frac{1}{f_0}. \tag{14}$$

Let $s(t)$ be a time-continuous signal. The signal spectrum $S(f)$ and the time signal $s(t)$ are related to each other via the Fourier integral and the inverse Fourier integral [59]

$$s(t) = \int_{-\infty}^{\infty} S(f) \mathrm{e}^{2\pi j f t} df, \tag{15a}$$

$$S(f) = \int_{-\infty}^{\infty} s(t) \mathrm{e}^{-2\pi j f t} dt. \tag{15b}$$

For the symbolic notation of a pair of Fourier transforms the correspondence symbol $\circ\!\!-\!\!\bullet$ is introduced in (6). The time-discrete signal $x[n]$ is given by

$$\mathsf{s}[n] = s(n\Delta t)\,. \tag{16}$$

In the following we discuss the fundamentals of signal sampling, analog-to-digital conversion, and digital signal processing.

For the representation of line spectra the delta distribution may be used in frequency domain. We note the following relations [59]:

$$1 \quad \circ\!\!-\!\!\bullet \quad \delta(f), \tag{17a}$$

$$\mathrm{e}^{j\omega_0 t} \quad \circ\!\!-\!\!\bullet \quad \delta(f - f_0), \tag{17b}$$

$$\cos\omega_0 t \quad \circ\!\!-\!\!\bullet \quad \frac{1}{2}\left[\delta(f + f_0) + \delta(f - f_0)\right], \tag{17c}$$

$$\sin\omega_0 t \quad \circ\!\!-\!\!\bullet \quad \frac{j}{2}\left[\delta(f + f_0) - \delta(f - f_0)\right], \tag{17d}$$

where $\delta(x)$ is the Delta distribution with the property

$$f(x) = \int_{-\infty}^{\infty} f(x_1)\delta(x_1 - x)dx_1\,. \tag{18}$$

Using the delta distribution we may also represent the Fourier transforms of harmonic signals.

We consider a periodic sequence of Dirac pulses with period width T_0 and pulse area a according to Figure 7 (a) given by

$$s_A(t) = a \sum_{n=-\infty}^{\infty} \delta(t - n\Delta t_s) = \frac{a}{\Delta t_s} \mathrm{III}\left(\frac{t}{\Delta t_s}\right), \tag{19}$$

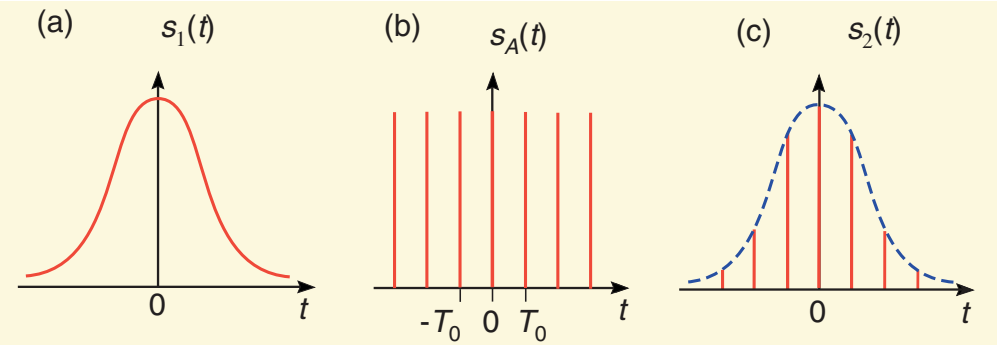

Figure 8: (a) Input signal, (b) Sampling signal, (c) Sampled signal.

where $\text{Ш}(x)$ is the normalized *sampling function* defined by

$$\text{Ш}(x) = \sum_{n=-\infty}^{\infty} \delta(x-n) = \sum_{n=-\infty}^{\infty} \mathrm{e}^{2\pi jnx}\,. \tag{20}$$

The symbol Ш is the cyrillic letter "shah". The sampling function has the property

$$\text{Ш}(t) \circ\!\!-\!\!\bullet\, \text{Ш}(f), \tag{21}$$

i.e. it is identical with its Fourier transform. From this it follows

$$\text{Ш}\left(\frac{t}{\Delta t_s}\right) \circ\!\!-\!\!\bullet\, \Delta t_s \text{Ш}(\Delta t_s f). \tag{22}$$

The spectrum $S_A(f)$ of $s_A(t)$, related to the time signal by

$$s_A(t) \circ\!\!-\!\!\bullet\, \Delta t_s S_A(f)\,, \tag{23}$$

is given by

$$S_A(f) = af_0 \sum_{n=-\infty}^{\infty} \delta(f-nf_0) = a\text{Ш}\left(\frac{f}{f_0}\right). \tag{24}$$

Figure 7 shows the time function $s_A(t)$ and the spectrum $S_A(f)$ of the sampling function with frequency f_0.

Sampling a time-continuous signal $s_1(t)$ in intervals Δt_s may be described by multiplying $s_1(t)$ with the sampling signal $s_A(t)$ given in (19). With (16), this yields

$$s_2(t) = s_A(t)s_1(t) = a \sum_{n=-\infty}^{\infty} s[n]\delta(t-n\Delta t_s)\,. \tag{25}$$

Figure 8 shows the signal $s_1(t)$, the sampling signal $s_A(t)$, and the sampled signal $s_2(t)$. The multiplication in time-domain, given in (25), corresponds to the convolution in frequency domain

$$s_2(t) = s_A(t)s_1(t) \quad \circ\!\!-\!\!\bullet\, \quad S_2(f) = S_A(f) \otimes S_1(f), \tag{26}$$

where $\otimes$ denotes the convolution operation, defined by

$$S_A(f) \otimes S_1(f) = \int_{\infty}^{\infty} S_A(f_1)S_1(f-f_1)df_1\,. \tag{27}$$

This yields

$$S_2(f) = \sum_{n=-\infty}^{\infty} \int_{-\infty}^{\infty} S_1(f-f_1)\delta(f_1-nf_0)\mathrm{d}f_1 = \sum_{n=-\infty}^{\infty} S_1(f-nf_0)\,. \tag{28}$$

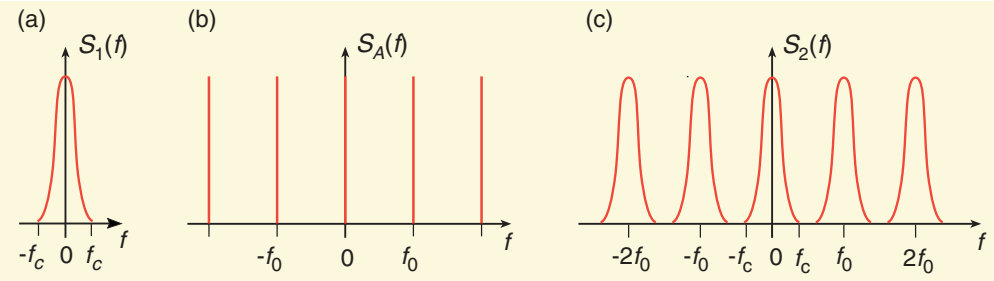

Figure 9: (a) Input signal spectrum, (b) Sampling signal spectrum, (c) Spectrum of sampled signal.

Figure 9 shows the spectrum $S_1(f)$ of the input signal, the spectrum $S_A(f)$ of the sampling signal, and the spectrum $S_2(f)$ of the sampled signal. The spectrum of the sampled signal is the periodic continuation of the spectrum of the input signal. The frequency spectrum of $s(t)$ has a width $[-f_c, f_c]$ and f_c is smaller than half of the sampling frequency f_0, i.e.

$$f_c < \frac{f_0}{2}\,. \tag{29}$$

In this case the periodically continued spectrum $S_2(f)$ does not overlap with the original spectrum $S_1(f)$. Therefore, by band limitation of $S_2(f)$ within an interval $[-f_{c1}, f_{c1}]$, with $f_c < f_{c1} \leq f_0/2$, we obtain the original signal with the spectrum $S_1(f)$. The frequency f_c is referred to as the *Nyquist frequency* [60]

A low-pass filter with rectangular characteristic and the cut-off frequency $f_0/2$ according to (29) exhibits the transfer function

$$H(f) = \Pi(f/f_0), \tag{30}$$

where $\Pi(x)$ is the rectangular *unit pulse function*, defined as

$$\Pi(x) = \begin{cases} 1 & \text{for} |x| \leq 1/2 \\ 0 & \text{for} |x| > 1/2 \end{cases}\,. \tag{31}$$

The Fourier transform of the pulse function is the sinc function, represented by

$$\mathrm{sinc}(x) = \frac{\sin x}{x}\,. \tag{32}$$

The spectrum of a rectangular pulse signal is given by the sinc function and vice versa, the pulse response of a rectangular signal transfer function is given by the sinc function:

$$\mathrm{sinc}(\pi f/f_0) \quad \bullet\!\!-\!\!\circ \quad f_0 \Pi(f_0 t)\,, \tag{33a}$$

$$\Pi(f/f_0) \quad \bullet\!\!-\!\!\circ \quad f_0\,\mathrm{sinc}(\pi f_0 t)\,. \tag{33b}$$

Figure 10 shows a rectangular transfer function the corresponding pulse response.

By band limitation of the sampled signal $s_2(t)$ to the frequency interval $[-f_0/2, f_0/2]$ we obtain the original time-continuous signal $s_1(t)$. This can easily be seen from (28) and (30). We obtain

$$S_1(f) = \Pi(f/f_0) S_2(f) \tag{34}$$

and with (33b)

$$s_1(t) = f_0\,\mathrm{sinc}(\pi f_0 t) \otimes s_2(t)\,. \tag{35}$$

After inserting (25) we find

$$s_1(t) = \sum_{n=-\infty}^{\infty} s[n]\,\mathrm{sinc}(\pi(f_0 t - n\Delta t_s))\,. \tag{36}$$

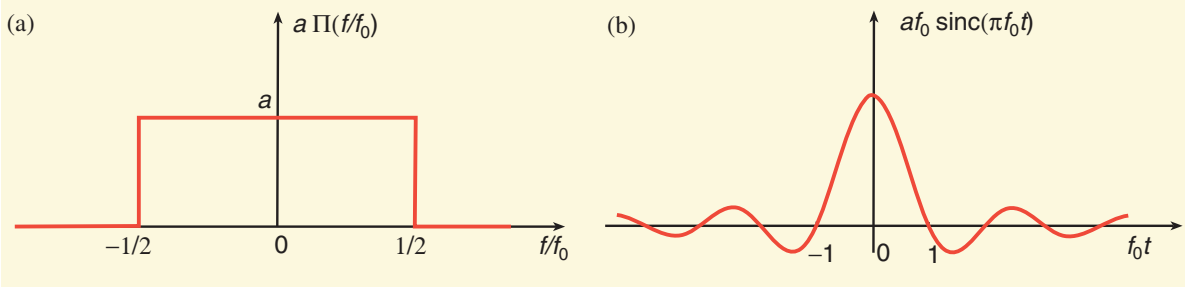

Figure 10: (a) Rectangular transfer function, (b) Pulse response.

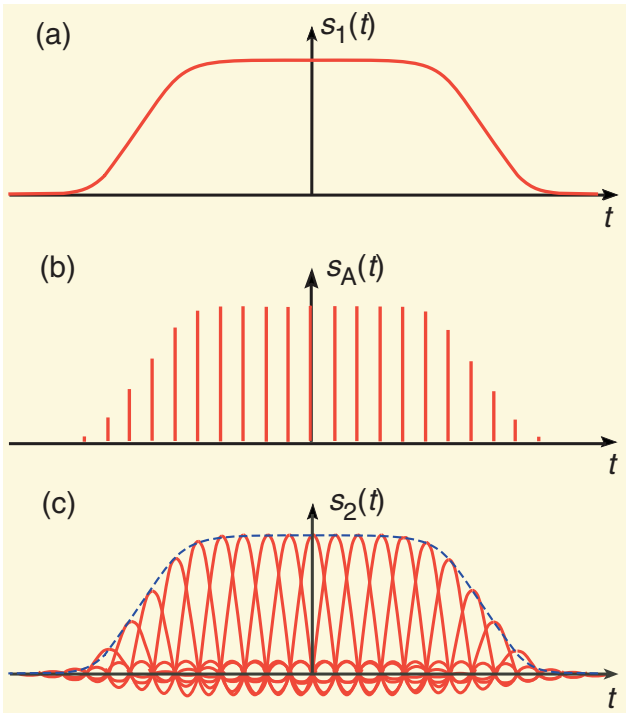

Figure 11: Signal sampling and reconstruction: (a) Band limited signal, (b) Sampled signal, (c) Reconstruction.

The ideal low-pass filter interpolates between the impulses of the discrete-time signal and reconstructs the continuous-time signal. An ideal low-pass filter is a discrete-to-continuous converter. We can formulate the sampling theorem: *A signal, band-limited with a cut-off frequency f_c, is completely determined by discrete samples taken at a sampling frequency $f_0 > 2f_c$ and may be restored completely.* Figure 11 shows the sampling of a band-limited signal and the subsequent signal reconstruction by band-limitation.

If we deal with real-world measured signals, we are performing the measurement over a time-interval of finite length. If a time sample of length T_0 is taken, we can describe this by a window function. Figure 12 shows rectangular and Gaussian window functions. Taking a segment of the signal $s_1(t)$ in the time interval $[\tau - T_0/2, \tau + T_0/2]$ can be described by multiplying $s_1(t)$ with the rectangular window function $\Pi((t - \tau)/T_0)$. By this we obtain the windowed signal

$$s_{1w}(t, \tau) = \Pi\left(\frac{t - \tau}{T_0}\right) s_1(t), \tag{37}$$

where τ is the time shift of the window. The rectangular time-windowing of the signal yields a convolution

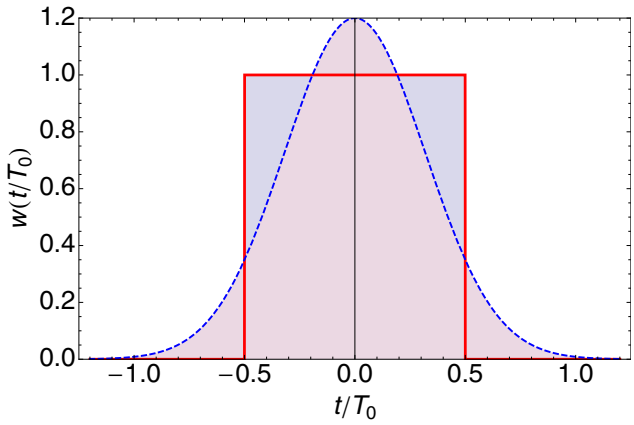

Figure 12: —— Rectangular window function, - - - - Gaussian window function.

of the signal spectrum with the transfer function $T_0 \operatorname{sinc}(\pi f T_0)$. Hence, we obtain

$$S_{1w}(f,\tau) = T_0 \left[\mathrm{e}^{-2\pi j f \tau} \operatorname{sinc}(\pi f T_0)\right] \otimes S_1(f)\,. \tag{38}$$

The spectrum $S_{1w}(f,\tau)$ depends on the position τ of the time window and is called *short-time Fourier transform* (STFT) [61, pp. 636-747].

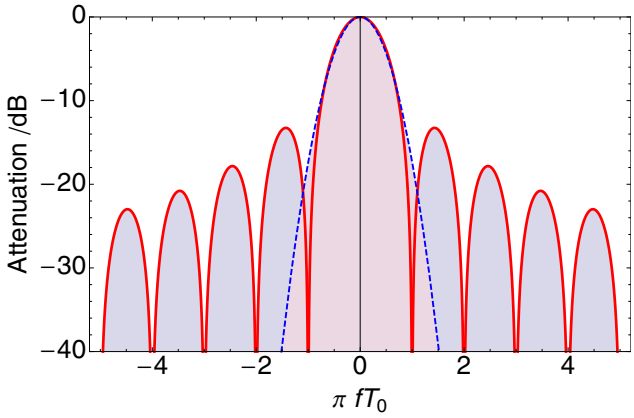

Figure 13: —— sinc transfer function, - - - - Gaussian transfer function.

Figure 13 shows the logarithmic plot of the magnitude of the transfer function $T_0 \operatorname{sinc}(\pi f T_0)$. The convolution with the sinc function yields a spectral broadening effect since the spectral lines are replaced by the sinc function. Rectangular time windowing yields a leaking out of spectral energy into other spectral regions due to the filtering. Therefore this effect is called *spectral leakage*.

Spectral leakage can be reduced by a smooth time windowing, where the window function exhibits a maximum value in the center of the window and goes smoothly down to zero at the boundaries of the window. The use of a Gaussian window will be an optimum choice in many cases since the Fourier transform of the Gauss function is also a Gauss function,

$$\mathrm{e}^{-\frac{t^2}{2T_0^2}} \quad \circ\!\!-\!\!\bullet \quad \sqrt{2\pi} T_0 \mathrm{e}^{-2\pi^2 f^2 T_0^2}. \tag{39}$$

The signal function windowed by a Gauss function $s_{2w}(t,\tau)$ and its spectrum $S_{2w}(f,\tau)$ are given by

$$s_{2w}(t,\tau) = \mathrm{e}^{-\frac{(t-\tau)^2}{2T_0^2}} s_1(t), \tag{40a}$$

$$S_{2w}(f,\tau) = \sqrt{2\pi} T_0 \left[\mathrm{e}^{-2\pi^2 f^2 T_0^2 - 2\pi j f \tau}\right] \otimes S_1(f). \tag{40b}$$

Figure 12 also shows a Gaussian window function, and in Fig. 13 the corresponding Gaussian signal transfer function is depicted. The bandwidth of the transfer function is inversely proportional to the width of the time window. Different from the case of a rectangular window function, the Gaussian window function yields a signal transfer function without side lobes and therefore only little spectral spreading. However, applying a Gaussian time window requires the use of a broader sample of the time signal in order to achieve the same bandwidth as with a rectangular window.

We can consider $s_{1w}(t,\tau)$ as a segment of a time-periodic signal with time period T_0. By convolution of $s_{1w}(t,\tau)$ with $T_0^{-1}\text{Ш}(t/T_0)$ we obtain with (20) the time-periodic signal

$$s_{1wp}(t,\tau) = T_0^{-1}\text{Ш}(t/T_0) \otimes s_{1w}(t,\tau) = \sum_{n=-\infty}^{\infty} s_{1w}(t - T_0, \tau). \tag{41}$$

With (33a) we obtain the spectrum of this periodically continued signal

$$S_{1wp}(f,\tau) = \text{Ш}\,(fT_0)\, S_{1w}(f,\tau)\,. \tag{42}$$

Since $s_{1wp}(t,\tau)$ is a periodic signal with period T_0, its spectrum $S_{1wp}(f,\tau)$ is a discrete spectrum with spectral line spacing $\Delta f = T_0^{-1}$.

We summarize that a signal, frequency limited with a frequency f_c, can be sampled with a sampling frequency $f_0 > 2f_c$, i.e. with sampling intervals $\Delta t = 1/f_0$ with no loss of information. The sampling process yields a periodic continuation of the basis band spectrum with the period f_0. If the Nyquist condition $f_0 > 2f_c$ is fulfilled this periodic spectrum continuation does not overlap with the base band of the original signal and can be removed by low-pass filtering. The low-pass filtering broadens the pulses of the sampled signal and reconstructs the time continuous signal. Furthermore, if the signal is bounded in time within an interval of length T_0, we can consider this signal as one period of a periodic signal with period T_0. This yields a discretization of the frequency spectrum with a spectral line spacing $\Delta f = T_0^{-1}$. We therefore can discretize a band-limited signal of finite length in time and frequency. Strictly speaking, due to the theory of Fourier transformation, a signal can either be limited in frequency or in time. However by appropriate time-windowing of band-limited signals with smooth window functions we can discretize finite segments of band-limited signals with little loss of information. This allows us to apply discrete Fourier transformation (DFT) for signal analysis. If the continuous spectrum is substituted in the DFT by a discrete spectrum, one sees a spectrum like a picket fence. The frequencies in between have to be interpolated.

6.2 Power Spectra of Random Signals

EMI signals, either due to their physical nature or due to the lack of knowledge of them, have to be considered as stochastic signals. Stationary stochastic signals cannot be described by amplitude spectra. We can compute an amplitude spectrum of a signal sample of finite length. However, since the phase in the spectrum of this sample will be random this amplitude spectrum will not characterize the complete stationary signal [62–65]. However, for certain quantities of stochastic signals *expectation values* can be given. Expectation values are defined as statistical average over a large ensemble of identical objects. In practice, often only a single object is accessible for measurements. In that case, the sample value can be taken from a single object at times separated by intervals large enough so that the measurements can be considered to be independent from each other. A process is called stationary if the ensemble averages are independent from time. Stationarity can be validated by time-sequential measurements, when a large number of signal samples of lengths T_1 are taken within a time interval $T_2 \gg T_1$ and the ensemble averages are computed within time intervals T_2. Now, within a time interval $T_3 \gg T_2$, several ensemble averages can be computed. If these ensemble averages converge to the same value with increasing length of the time intervals, the process may be considered stationary.

We can define the autocorrelation function $c(\tau)$ of stationary random signals $s_i(t)$ and $s_j(t)$ by

$$c_{ij}(\tau) = \langle s_i(t) s_j(t-\tau) \rangle. \tag{43}$$

The brackets denote the statistical ensemble average. For $i = j$ the function $c_{ii}(\tau)$ is called the *autocorrelation function* and for $i \neq j$ the function $c_{ij}(\tau)$ is called the *cross correlation function*. The mathematical definition of the exact ensemble average refers to an infinite ensemble. By taking the ensemble average over a finite ensemble with increasing ensemble element number, it should converge to the exact value. The assumption of stationarity means that the statistical average is independent of t. For stationary signals the statistical average can also be taken in time by

$$c(\tau) = \lim_{T\to\infty} \frac{1}{T} \int_{-T/2}^{T/2} s(t)s(t-\tau)dt. \tag{44}$$

The correlation function for two different signals ($i \neq j$) is named *cross correlation function*. Substituting t by $t + \tau$ in (44) yields

$$c_{ij}(\tau) = c_{ji}(-\tau)\ . \tag{45}$$

From this it follows that the autocorrelation function is symmetric, i.e. $c_{ii}(\tau) = c_{ii}(-\tau)$.

Let us now investigate which statements can be made concerning the spectrum of a random signal. Since a stationary noise signal is not decaying for $t \to \infty$, the noise signal is not square integrable or absolute integrable and therefore an amplitude spectrum of a stationary noise signal does not exist. However, we can consider a sample of a noise signal with finite extension in time. Let us consider the segment $s_T(t)$ of the stationary noise signal $s(t)$. This segment is given by

$$s_T(t) = \begin{cases} s(t) & \text{for} \quad -\frac{T}{2} < t < \frac{T}{2} \\ 0 & \text{for} \quad |t| \geq \frac{T}{2} \end{cases}\ . \tag{46}$$

We call the signal $s_T(t)$ the time-windowed signal. In general the Fourier transform $S_T(f)$ of the time-windowed signal $s_T(t)$ exists and is given by

$$S_T(f) \bullet\!\!-\!\!\circ\, s_T(t)\ . \tag{47}$$

With (44) and (46) we can represent the correlation function $c_{ij}(\tau)$ also by

$$c_{ij} = \lim_{T\to\infty} \frac{1}{T} \int_{-\infty}^{\infty} s_{iT}(t)s_{jT}(t-\tau)\ dt\,. \tag{48}$$

For $T \to \infty$, the integrals (44) and (48) become equal. We express $s_{iT}(t)$ via its Fourier spectrum and obtain

$$c_{ij}(\tau) = \lim_{T\to\infty} \frac{1}{T} \int_{-\infty}^{\infty} \left[\int_{-\infty}^{\infty} S_{iT}(f)\mathrm{e}^{2\pi jft}\ df \right] s_{jT}(t-\tau)\ dt\,. \tag{49}$$

After interchanging the sequence of both integrations and substituting $t - \tau = t'$, $dt = dt'$, we obtain

$$c_{ij} = \lim_{T\to\infty} \frac{1}{T} \int_{-\infty}^{\infty} S_{iT}(f)\mathrm{e}^{2\pi jf\tau} \left[\int_{-\infty}^{\infty} s_{jT}(t')\mathrm{e}^{2\pi jft'}\ dt' \right]\ df\,, \tag{50}$$

where the second integral yields $S^*_{jT}(f)$, so that we obtain

$$c_{ij}(\tau) = \lim_{T\to\infty} \frac{1}{T} \int_{-\infty}^{\infty} S_{iT}(f)S^*_{jT}(f)\mathrm{e}^{s\pi jft}\ df\,. \tag{51}$$

The limit process $T \to \infty$ in general cannot be interchanged with the integration. Since the spectra $S_{iT}(f)$ are not existing for $T \to \infty$. Since $c_{ij}(t)$ according to (43) is an ensemble average, we also can apply the evaluation of the ensemble average to the right side of (51) and we may interchange the sequence of integration and ensemble averaging. For the ensemble average of the product $S_{iT}(f)S^*_{jT}(f)$ in general the limit

$$C_{ij}(f) = \lim_{T\to\infty} \frac{1}{T} <S_{iT}(f)S^*_{jT}(f)> \tag{52}$$

exists. Therefore, after forming the ensemble average integration and the limit process in (51) may be interchanged. $C_{ij}(f)$ is the Fourier transform of the correlation function.

$$C_{ij}(f) \bullet\!\!-\!\!\circ\, c_{ij}(\tau) \;, \tag{53}$$

$$C_{ij}(f) = \int_{-\infty}^{\infty} c_{ij}(\tau) \mathrm{e}^{-2\pi j f \tau} \; d\tau \;, \tag{54}$$

$$c_{ij}(\tau) = \int_{-\infty}^{\infty} C_{ij}(f) \mathrm{e}^{2\pi j f \tau} \; df \;. \tag{55}$$

The function $C_{ij}(f)$ is named the *correlation spectrum*. For $i = j$ the correlation spectrum $C_{ii}(f)$ is called the *autocorrelation spectrum*, and for $i \neq j$ the correlation spectrum is called the *cross correlation spectrum*.

From (54) it follows

$$C_{ij}(f) = C_{ji}^{*}(f) \;. \tag{56}$$

For real time functions of the signals, $s_i(t)$ and $s_j(t)$ the real part of $C_{ij}(f)$ is symmetric and its imaginary part is antisymmetric. The autocorrelation spectrum $C_{ii}(f)$ is real and symmetric.

From(55) follows, that the autocorrelation spectrum integrated over the whole frequency domain yields the variance of the signal:

$$\int_{-\infty}^{\infty} C_{ii}(f) \; df = c_{ii}(0) = \sigma_i^2 \;. \tag{57}$$

The variance σ_i^2 of the random signal $s_i(t)$ in the frequency interval $[f, f + df]$ is given by

$$\sigma_i^2 = 2C_{ii}(f) \; df \;. \tag{58}$$

7 Digital Signal Processing

7.1 Digital Fourier Transformation

To evaluate the signal spectrum, a digitized signal $\mathsf{s}[n]$ is further processed by *Digital Fourier Transform (DFT)*. Computationally efficient DFT algorithms exist for computation of the Fourier transform at N equally spaced frequency values from N equally spaced time samples [59, 60, 66–69]. These algorithms are called *Fast Fourier Transformation* (FFT) algorithms. Consider a discrete time sequence of a sampled signal $\mathsf{s}[n]$, where n is integer and $\mathsf{s}[n]$ is periodic with N, so that $\mathsf{s}[n + N] = \mathsf{s}[n]$.

The discrete-time signal function $\mathsf{s}[n]$ is related to the continuous-time signal function $s(t)$ of length T_0 by

$$\mathsf{s}[n] = s(n\Delta t) \quad \text{with } T_0 = N\Delta t, \tag{59}$$

where Δt is the sampling interval. The discrete-frequency spectrum $\mathsf{S}[k]$ is related to the continuous-frequency spectrum $\mathsf{S}(f)$ by

$$\mathsf{S}[k] = S(k\Delta f), \tag{60}$$

where k is integer Δf is the spacing of the spectral lines. The quantities N, T_0, Δt, and Δf are related by

$$\Delta f = \frac{N}{T_0}. \tag{61}$$

The discrete Fourier transform (DFT) is given by

$$\mathsf{S}[k] = \sum_{n=0}^{N-1} \mathsf{s}[n] \exp\left(-2\pi j \frac{nk}{N}\right). \tag{62}$$

In the spectrum $\mathsf{S}[k]$, the term $\mathsf{S}[0]$ is the DC mean value of $x[n]$. The Nyquist frequency k_{Nyq} is given by

$$k_{Nyq} = \begin{cases} \frac{N}{2} & \text{for even} \quad N \\ \frac{N+1}{2} & \text{for odd} \quad N \end{cases} . \tag{63}$$

Since $\mathsf{S}[k]$ is periodic in k with period N, the frequencies $0 < k < k_{Nyq}$ are the positive frequencies, whereas $k_{Nyq} \leq k < N$ correspond to the negative frequencies.

The discrete Fourier transform $\mathsf{S}[k]$ has integer arguments k and is also periodic with N. The inverse discrete Fourier transform is given by

$$\mathsf{s}[n] = \frac{1}{N} \sum_{k=0}^{N-1} \mathsf{S}[k] \exp\left(2\pi j \frac{nk}{N}\right) . \tag{64}$$

For the case where N is an integer power of 2, i.e. $N = 2^l$ with integer l, very efficient FFT algorithms are available [59, 60, 67–70].

The spectral estimation is performed on the basis of the DFT under the assumption that the $\mathsf{s}[n]$ is periodic in n with a period N. However, $\mathsf{s}[n]$ is not really periodic since we only have periodically continued measured signal sequence of length N. To avoid spectral leakage the time record $\mathsf{s}[n]$ needs to be multiplied with a window function $\mathsf{w}[n]$ which exhibits a maximum value for $n = N/2$ and smoothly goes to zero for n approaching 0 or $N - 1$, respectively [22, 28],

$$\mathsf{s}_w[n] = \mathsf{w}[n]\, \mathsf{s}[n] . \tag{65}$$

In the frequency domain this yields a convolution

$$\mathsf{S}_w[k] = \mathsf{W}[k] \otimes \mathsf{S}[k] . \tag{66}$$

where the time-discrete convolution of two signals $\mathsf{S}_a[k]$ and $\mathsf{S}_b[k]$ is given by [60]

$$\mathsf{S}_a[k] \otimes \mathsf{S}_b[k] = \sum_{m=0}^{N-1} \mathsf{S}_a[((l))_N] \mathsf{S}_b[((k-l))_N], \tag{67}$$

The notation $((n))_{mod\, N}$ means "n *modulo* N", i.e. $((n))_{mod\, N} \in [0, N-1]$ and $((n))_{mod\, N} - n$ is an integer multiple of N. According to this definition $\mathsf{s}[n, m]$ in the interval $[n \in [0, N-1]$ is a sample taken from $\mathsf{s}[n]$ in the interval $[n \in [m, m+N-1]$.

A Gaussian window function

$$\mathsf{w}[n] = \frac{1}{G_C N} \exp\left[-\frac{1}{2}\left(\frac{\pi}{\sqrt{2 \ln 2} B_{IF} T_0 n}\right)^2\right] \tag{68}$$

is used, where the coherent gain G_C is a scaling factor to compensate for the signal energy loss due to the windowing [66]. It is given by

$$G_C = \frac{1}{N} \sum_{n=0}^{N-1} \mathsf{w}[n] . \tag{69}$$

7.2 Digital Signal Processing with Periodogram

The *periodogram* is an estimation of the spectral density of a signal. It is an efficient tool for the Fourier analysis of stationary random signals [60, pp. 730-754], [71, pp. 393-426], [61, pp.616-618]. The periodogram method was first published by Bartlett [72]. In Bartlett's method the data is smoothed by averaging over

the power computed for a number P of short-time signal segments. Welch has combined DFT methods with the use of a data window and developed a method for averaging of short, modified periodograms [73]. The periodogram method exploits the short-time Fourier transformation (STFT) for spectral estimation using a window function. The STFT is a time-dependent Fourier transformation since it depends on the position of the time window.

Consider a time-discrete signal $s[n]$ of infinite extension in time, i.e. with $n = -\infty \cdots -2, -1, 0, 1, 2, \ldots \infty$. By multiplying with a window function $w[n]$ of length $N-1$ we obtain the time windowed function

$$s[n, m] = s[((n))_{mod\, N} + m]w[n], \tag{70}$$

where $((n))_{mod\, N}$ means n *modulo* N. Outside the interval $[n \in [0, N-1]$ the function $s[n, m]$ is periodically continued.

Following (62), the STFT $S[k, m]$ of a signal $s[n]$ is defined as

$$S[k, m] = \frac{1}{N} \sum_{n=0}^{N-1} s[n, m] \exp\left(-2\pi j \frac{nk}{N}\right), \tag{71}$$

where $w[n]$ is the time window, and the discrete time coordinate m indicates the amount of shift in the time window. If the window has a finite length N, the Fourier transform needs to be performed over this window length only. Due to the time windowing of the signal, the spectrum $S[k, m]$ can be taken for various delays m. However, due to the statistical distribution of the phases in the spectral samples taken at different times, the mean spectrum will be zero and the spectrum does not provide a useful characterization of the random signal. We can reconstruct the continuous amplitude spectrum $S(f, m)$ of the finite-time signal segment by substituting in (71) $k/N \to fT$. This yields

$$S(f, m) = \frac{1}{N} \sum_{n=0}^{N-1} s[n, m] \exp\left(-2\pi jnfT\right). \tag{72}$$

Figure 14 shows as an example the STFT of the main EMI burst at the electric start of a combustion engine [22]. The measurement of the radiated EMI during the electric start of a combustion engine impressively demonstrates the advantages of time-domain EMI measurement techniques which allow us to measure short-time EMI events and to obtain complete information about the EMI spectrum. The recorded frequencies were limited to the frequency band of FM radio from 88 MHz to 108 MHz. In that special case, maximum interference was found at 104.3125 MHz.

When the signal under consideration is generated by a stationary random process, it can be characterized by averaged quantities such as the mean value and the variance. The mean value of a signal segment with length N, the *sample mean*, represented by $s[n]$, is given by

$$\langle s[m] \rangle = \frac{1}{N} \sum_{n=0}^{N-1} s[n, m]. \tag{73}$$

The mean value of the signal represents its DC level. The *sample variance* of the considered signal segment is

$$\sigma_s^2[m] = \langle (s[n, m] - \langle s \rangle [m])^2 \rangle = \frac{1}{N} \sum_{n=0}^{N-1} (s[n, m] - \langle s \rangle [m])^2. \tag{74}$$

Let us consider the *time-discrete autocorrelation function* of the signal si[n], given by

$$c[n, m] = \frac{1}{N} \sum_{n=0}^{N-1} s[n + m] s^*[m]. \tag{75}$$

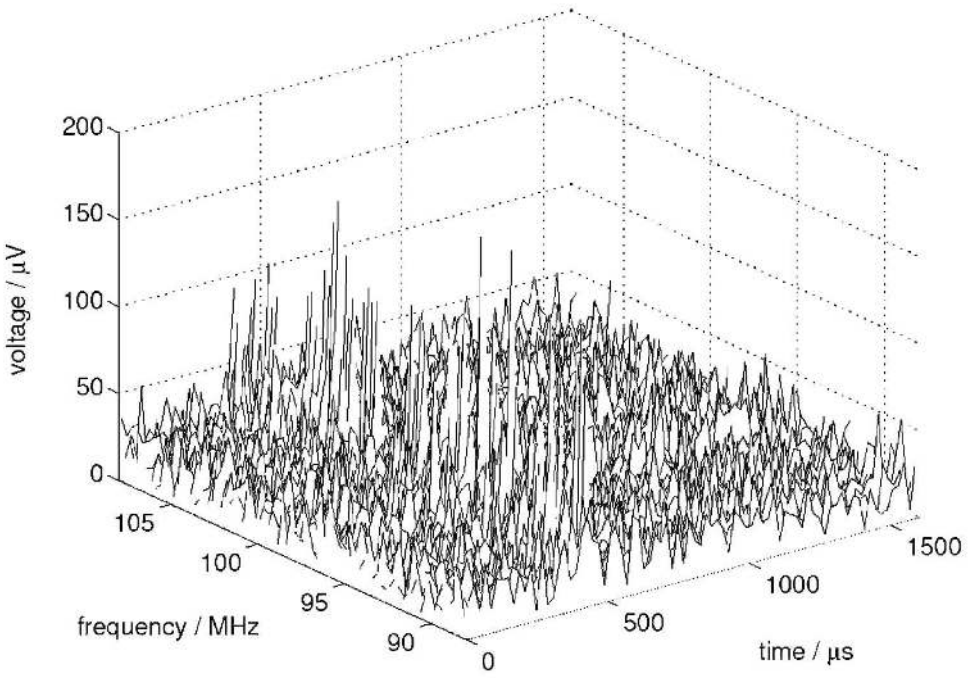

Figure 14: STFT of the main EMI burst at the electric start of a combustion engine [74].

The superscript * denotes the complex conjugate. However, usually we have to deal with real time signals. In order to ensure that the values of $s[n]$ outside the interval $[0, N-1]$ are excluded, we modify this equation as follows:

$$c[n,m] = \frac{1}{N} \sum_{n=0}^{N-1-n} s[n+m]s^*[m]. \tag{76}$$

Different from the signal amplitudes, the correlation functions converge to non-vanishing limit values when averaged over samples with various time delays m.

Applying the STFT, defined in (71), we obtain the *frequency-discrete autocorrelation spectrum*

$$C[k,m] = \frac{1}{N} \sum_{n=0}^{N-1} c[n,m] \exp\left(-2\pi j \frac{nk}{N}\right) \tag{77}$$

of the signal sample taken at a time shift m. The autocorrelation spectrum also can be represented as the absolute square of the short-time Fourier spectrum $S[k,m]$ given in (71),

$$C[k,m] = \frac{1}{N} S[k,m]S^*[k,m]. \tag{78}$$

We can reconstruct the continuous autocorrelation spectrum $C(f,m)$ of the finite-time signal segment by replacing in (77) or (78), respectively, $k/N \to fT$. From (72) and (77) we obtain

$$C[f,m] = \frac{1}{N} \left|S[f,m]\right|^2. \tag{79}$$

This time-dependent short-time spectrum is called *periodogram*.

In the Bartlett method [72], the periodograms $C[f,m_p]$ are calculated for a number of P non-overlapping samples of the signal. The delays m_p, with $p = 0, 1, 2, \ldots P$, are spaced such that $m_{p+1} - m_p \geq N$. This

yields the *Bartlett periodogram* [66, 74]

$$P_B(f) = \frac{1}{PN} \sum_{p=0}^{P-1} \sum_{n=0}^{N-1} C[k, m_p] \mathrm{e}^{2\pi jkfT}. \tag{80}$$

The Bartlett periodogram can also be written as

$$P_B(f) = \frac{T}{PN} \sum_{p=0}^{P-1} \left| \sum_{n=0}^{N-1} s[n, m_p] \mathrm{e}^{-2\pi jnfT} \right|^2 \tag{81}$$

or, with (79), as

$$P_B(f) = \frac{1}{PN} \sum_{p=0}^{P-1} |S[f, m_p]|^2 . \tag{82}$$

The Bartlett averaging reduces the variance of the spectrum estimation by a factor of P, however, at the cost of a reduction of the frequency resolution by the same factor [75]. Welch has modified Bartlett's method by using windowed, time-overlapping data segments [73]. The Welch periodogram is given by

$$P_W(f) = \frac{T}{PU} \sum_{p=0}^{P-1} \left| \sum_{n=0}^{N-1} w[n] s[n, m_p] \mathrm{e}^{-2\pi jnfT} \right|^2 , \tag{83}$$

where $w[n]$ is the window function and U is the discrete-time window gain, given by

$$U = T \sum_{n=0}^{N-1} w^2[n] . \tag{84}$$

Figure 15 shows the comparison of the EMI spectra measured in the frequency range from 30 MHz to 1 GHz with a conventional EMI receiver and time-domain EMI measurement system [74]. The measurements were made in both cases in the average detector mode. The use of the Welch periodogram yielded a reduction of the noise floor by 8 dB, compared with the use of the Bartlett periodogram.

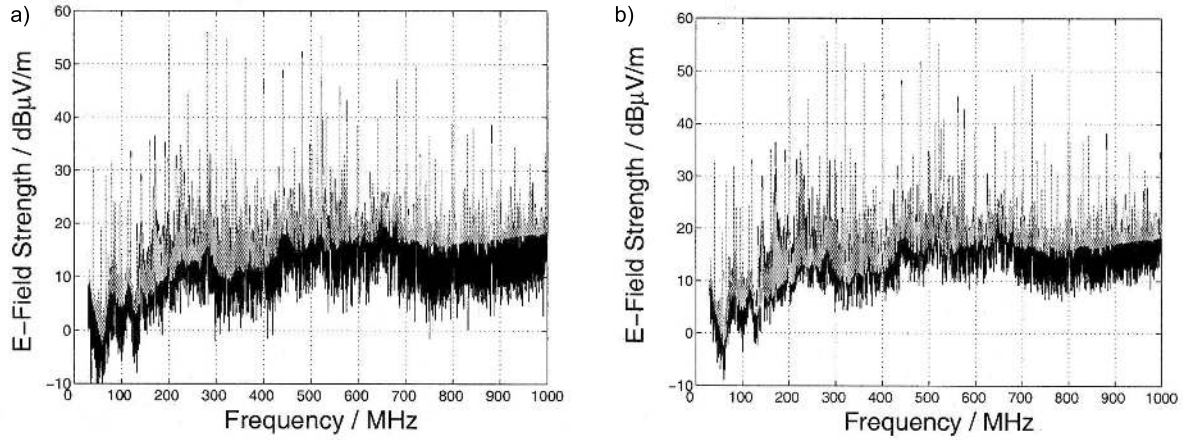

Figure 15: Comparison of periodogram (black line) and EMI receiver (grey line) for (a) Bartlett periodogram and (b) Welch periodogram [74].

7.3 The Signal-to-Noise Ratio

The signal-to-noise ratio SNR is defined as the ratio of signal power P_s to noise power P_n and usually is expressed in decibel

$$SNR = 10 \log_{10} \frac{P_s}{P_n} \text{ dB} = 20 \log_{10} \frac{\sigma_s}{\sigma_n} \text{ dB}\,, \tag{85}$$

where σ_s^2 is the variance of the signal $s(t)$, given by

$$\sigma_s^2 = \left\langle \left(s^2(t) - \langle s(t) \rangle^2 \right) \right\rangle \,. \tag{86}$$

The signal-to-noise ratio of a time-domain EMI measurement system is limited by the quantization noise. For quantizers which round the sample value to the closest quantization level, the amplitude of the quantization noise $e[n]$ is in the range

$$-\frac{\Delta}{2} < e[n] \leq \frac{\Delta}{2}\,, \tag{87}$$

where Δ is the quantization interval. Assuming that the random variable $e[n]$ is uniformly distributed over this interval, the mean value of $e[n]$ is zero and the variance is given by [60, p.120]

$$\sigma_e^2 = \frac{\Delta^2}{12}\,. \tag{88}$$

With a binary code of $B+1$ bits, we can code 2^{B+1} quantization levels. Let s_m be the maximum signal amplitude and consider that the signal can assume positive and negative sign. One bit is used for coding the sign and B bits are used for coding the magnitude of the signal. In that case the quantization interval is given by

$$\Delta = \frac{2 s_m}{2^{B+1}} = \frac{s_m}{2^B}\,. \tag{89}$$

From (85), (86), (88), and (89) we obtain

$$SNR = 10 \log_{10} \left(\frac{12 \cdot 2^{2B} \sigma_s^2}{s_m^2} \right) \text{dB} = \left[6.02B + 10.8 - 20 \log_{10} \left(\frac{s_m}{\sigma_s} \right) \right] \text{dB}\,. \tag{90}$$

The parameter s_m is fixed for a given ADC converter. The parameter σ_s is the rms value of the signal and will be necessarily smaller than s_m. For a sinus signal with maximum amplitude, for example, we obtain $\sigma_s = s_m/\sqrt{2}$.

Let $s[n]$ be the sampled but not yet amplitude quantized signal. The signal $s_1[n]$ is time-discrete and amplitude-continuous. After quantization of $s[n]$ we obtain the digitized signal $\tilde{s}[n]$. We can consider the the digitized signal as a superposition of the original signal $s[n]$ and the quantization noise $e[n]$,

$$s[n] = \tilde{s}[n] + e[n]. \tag{91}$$

Applying a time-window $w[n]$ to the sampled function yields the windowed function

$$s_w[n] = w[n] s[n] = w[n] \tilde{s}[n] + w[n] e[n]\,. \tag{92}$$

From (85), (86), (85), and (92) we obtain the average signal-to noise-ratio of the calculated spectrum [27,28] given by

$$SNR = \frac{\frac{1}{N} \sum_{n=0}^{N-1} \left(w[n] \tilde{s}[n] - \frac{1}{N} \sum_{m=0}^{N-1} w[m] \tilde{s}[m] \right)^2}{\frac{1}{N} \sum_{n=0}^{N-1} \left(w[n] e[n] - \frac{1}{N} \sum_{m=0}^{N-1} w[m] e[m] \right)^2}\,. \tag{93}$$

For $|e[n]| \ll \tilde{s}[m]$ we can replace $\tilde{s}[m]$ by $s[n]$ and obtain

$$SNR = \frac{\frac{1}{N} \sum_{n=0}^{N-1} \left(w[n] s[n] - \frac{1}{N} \sum_{m=0}^{N-1} w[m] s[m] \right)^2}{\frac{1}{N} \sum_{n=0}^{N-1} \left(w[n] e[n] - \frac{1}{N} \sum_{m=0}^{N-1} w[m] e[m] \right)^2}\,. \tag{94}$$

8 Modern Time-Domain Electromagnetic Interference Measurement Systems

8.1 The Time-Domain EMI Measurement System with one ADC

The first time-domain EMI measurement systems for the frequency range 30 MHz - 1 GHz have been described in [16, 17]. Figure 16 shows the block diagram of a time-domain EMI measurement system. The system can be applied for the measurement of radiated or conducted electromagnetic interference. For the measurement of radiated electromagnetic interference a broad-band antenna, for the measurement of conducted EMI either a current clamp or line impedance stabilization network (LISN) is used. In the EMI measurement system the incoming signal is first amplified and then low-pass filtered by the low-pass filter LPF, so that the signal fulfills the Nyquist condition, i.e. that it is band-limited with the Nyquist frequency f_c which, according to (29) is smaller than half the sampling frequency f_0. Then, in the analog-to digital converter ADC, the signal is converted into a digital signal and a block $s[n]$ of N signal samples is stored. Via the short-time fast Fourier transform (STFFT), using (62), the short-time spectrum $S_w[k]$ is computed. The periodograms are computed using (81) or (83), respectively.

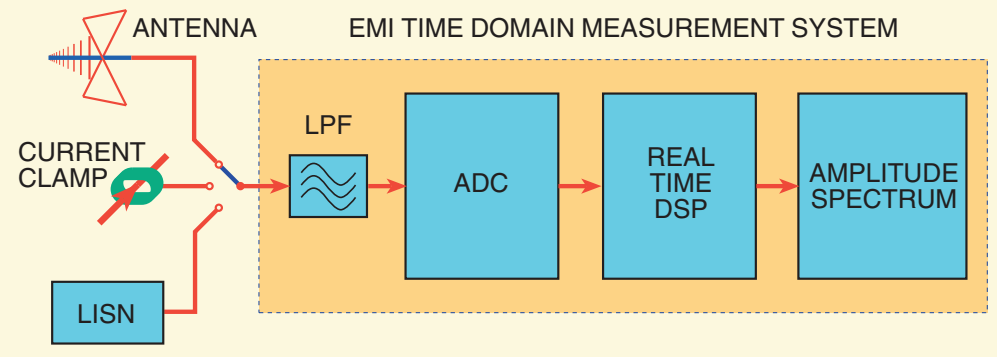

Figure 16: Time-domain EMI measurement system.

Further signal processing strategies for broad-band and narrowband signals have been discussed in [18, 19, 22]. To avoid spectral leakage the time signal blocks $s[n]$ are windowed with a window function $w[n]$ as described in Subsection 6.1, yielding the windowed signal block

$$s_w[n] = \frac{1}{G_C} w[n]\, s[n]\,, \tag{95}$$

where G_C is the coherent gain, defined in (69) [18] .

For the statistical averaging of the spectral samples only the magnitudes of the spectral amplitudes is used and the phase information is not further considered. We use the single-sided amplitude spectrum defined as

$$S_A[k] = \begin{cases} \frac{1}{N}|S_w[0]| & \text{for} \quad k = 0 \\ \frac{\sqrt{2}}{N}|S_w[k]| & \text{for} \quad 1 \le k < k_{Nyq} \end{cases}\,, \tag{96}$$

where k_{Nyq} is the Nyquist frequency defined in (63). We take only the spectral amplitudes up to the Nyquist frequency. The frequencies k above the Nyquist frequency, i.e. with $k_{Nyq} \le k < N$, correspond to the negative frequencies and the respective spectral amplitudes are conjugate complex to the spectral amplitudes in the region $1 \le k < k_{Nyq}$. So we have to take twice the spectral amplitudes in the region $1 \le k < k_{Nyq}$ and to divide them by $\sqrt{2}$ to account for the effective value.

For statistical averaging of multiple short-time spectra $S_A[k, p]$ with $p \in [0, P-1]$, the periodogram

$S_P^{avg}[k]$ is computed by averaging the spectral amplitude for each frequency bin, yielding

$$S_P^{avg}[k] = \frac{1}{P} \sum_{p=0}^{P-1} S_A[k,p] \,. \tag{97}$$

The RMS spectrum $S_P^{rms}[k]$ is obtained by

$$S_P^{rms}[k] = \sqrt{\frac{1}{P} \sum_{p=0}^{P-1} S_A^2[k,p]} \,. \tag{98}$$

The peak value spectrum $S_P^{peak}[k]$ is given by

$$S_P^{peak}[k] = \max S_A[k,p] \quad \text{for } p \in [0, P-1] \,. \tag{99}$$

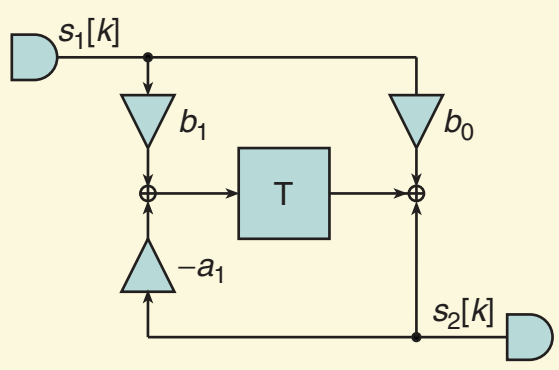

Figure 17: Signal fow in a digital IIR1 filter.

A time-domain measurement system that can evaluate spectra in the quasi-peak detector mode has been presented in [23,24]. To realize the discharge characteristics according to Figure 5 (b) a digital infinite impulse response (IIR) filter was implemented [68, pp. 621-664]. Figure 17 shows the signal flow characteristics of the digital IIR1 filter. Applying the bilinear transform

$$s = \frac{2}{\Delta t} \frac{z-1}{z+1t} \,, \tag{100}$$

where s is the complex frequency in the Laplace domain to the discharge transfer function $H(s)$ of the analog circuit in Figure 5 (b), given by

$$H(s) = \frac{1}{1 + s\tau_d} \,, \tag{101}$$

we obtain the IIR1 described by the signal flow characteristics given in Fig. 17.

The software implementation of the described detector modes facilitates the simultaneous evaluation of the peak, average and rms spectra.

The modeling of the IF-filter by a Gaussian window function has been presented in [18–28]. The system generates a statistical model from the EMI signal. This statistical model is used to reconstruct the virtual IF signal at each discrete spectral value. The IF signal is demodulated and evaluated by a digital quasi-peak detector. An improved version of the system for conducted emission measurements has been presented in [25].

8.2 A Low-Noise High-Dynamic Ultra-Broad-Band Time-Domain EMI Measurement System

The dynamic range of the TDEMI measurement system is limited by the resolution of the used ADCs. Today, high-speed ADCs with sampling rates beyond 2 GBit/s usually have a resolution of only 10 bit. According to (90) this would limit the signal-to-noise ratio for stationary signals between 60 dB and 70 dB. This would fulfill the requirements of CISPR 16-1. However, for transient or impulsive noise the SNR would be below 10 dB. The dynamics of a time-domain EMI measurement system can be considerably increased by using multiresolution analog-to-digital conversion [27, 28, 30, 34, 38, 76]. By several parallel analog-to-digital converters a multiresolution TDEMI measurement system has been developed that shows sufficient dynamic range to fulfill the international EMC standards CISPR 16-1-1 [39].

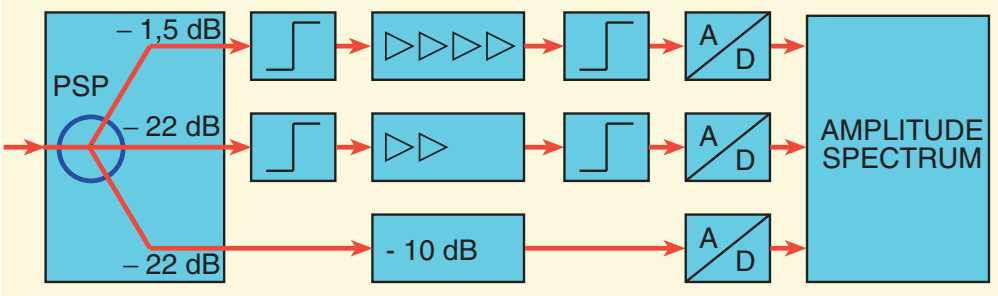

Figure 18: Block diagram of the multi-resolution time-domain EMI measurement system.

Figure 18 shows the block diagram of the multi-resolution time-domain EMI measurement system. The EMI input signal is split via the power splitter PSP into three channels. The first channel, which is the upper channel in Fig. 18, is the most sensitive channel. It digitizes the signals in the amplitude range from 0 V to 1.8 mV. The second channel is dedicated to the amplitude range from 0 V to 200 mV, and the third channel digitizes the signals in the amplitude range from 0 V to 10 V. The channels 1 and 2 have non-saturable diode limiters at the input so that these channels are not overloaded by signals exceeding their dedicated amplitude range. The system uses three 10 bit ADCs that operate with a sampling rate of 2.3 GS/s [34]. The digitized signals are processed in the digital signal processing unit by a Field Programmable Gate Array (FPGA) [33].

Using a polyphase decimator [60] the range from 30 MHz to 1 GHz is subdivided into eight frequency bands which are measured sequentially in real-time [33, 39]. Figure 19 shows the block diagram of the digital down-converter DDC unit. For the in-phase and quadrature channel a polyphase decimation filter reduces the sampling frequency in order to fulfill the Nyquist criterion. Every sub-band is digitally down-converted and the sub-bands are processed sequentially [30]. By the continuous processing via the STFFT a virtual IF-signal for a selectable frequency can be provided as requested by CISPR 16-1-1. The measurement time has been reduced by a factor of 2000 in comparison to measurements in frequency domain. It has been shown that a 16 bit fixed point operation of the STFFT is sufficient to fulfill the requirements according to the dynamic range. The requirements for full compliance measurements with the real-time time-domain EMI measurement system are discussed in [31]. A more detailed description of the hardware has been presented in [27, 34].

In [29–36] the suitability for full compliance measurements has been demonstrated. In [37, 38] a realtime time-domain EMI measurement system for automotive testing is reported. In this system a reduction of the measurement time by a factor of 8000 has been achieved. Automotive tests require dense frequency bins and small IF-bandwidth. In frequency domain such measurements take extremely long. Sometimes they would exceed the life-time of a component. With a numerical implementation of the 9 kHz IF filter, 8192 frequency bins can be calculated in parallel in real-time. A reduction of the measurement time by a factor of 8000 has been achieved. In [35] a test procedure based on an enhanced pre- and final scan has been presented. This

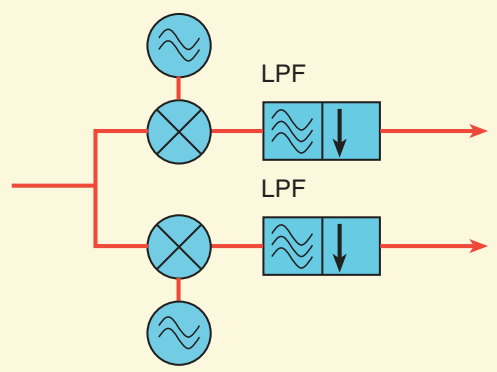

Figure 19: Digital down-conversion.

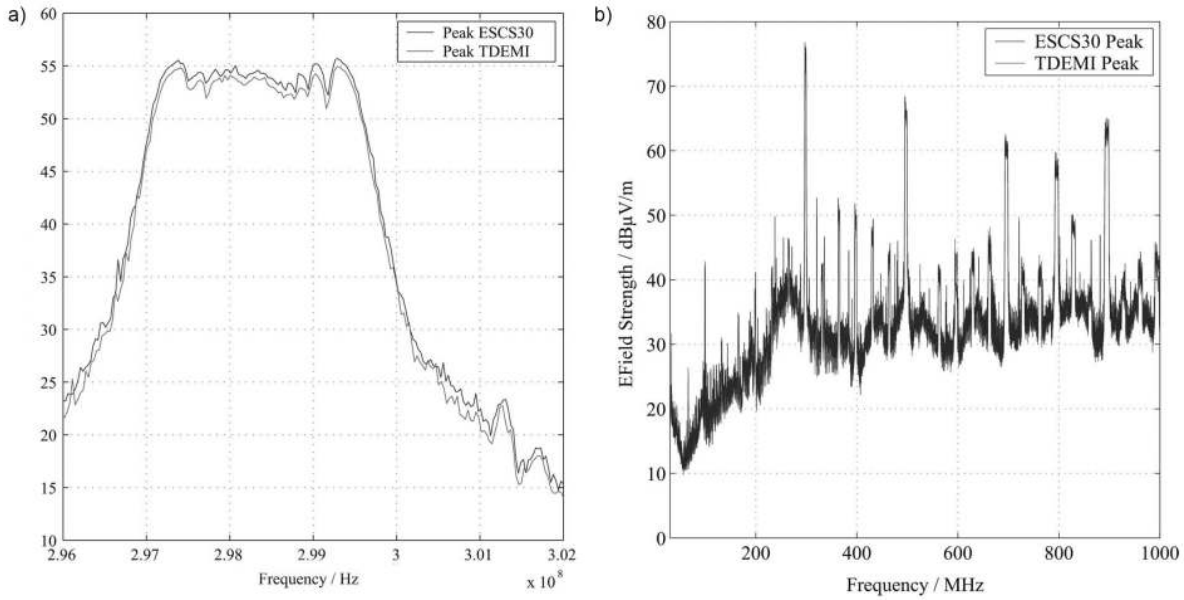

Figure 20: Radiated EMI of a desktop computer measured in the peak detector mode in the frequency intervals (a) 296–302 MHz, (b) 30 MHz to 1 GHz. [39].

procedure yields a further reduction of the test time by at least one order of magnitude.

The commercially available GAUSS Instruments TDEMI 1G® measurement system exhibits a frequency range of 9 kHz 1 GHz, the CISPR bandwidths 200 Hz, 9 kHz, 120 kHz, and 1 MHz, and a spurious free dynamic range of about 55 dB [77]. Compared with traditional EMI receivers the measurement time is reduced by a factor of 4000. In the quasi-peak mode the overall Measurement time for a single scan in the frequency range 30 MHz - 1 GHz takes about 2 minutes. Pre-scans are performed to detect only the critical frequencies, and to reduce the total scan time of the following final measurement. The time-domain EMI measurement system allows us to improve the quality of such prescans, because the pre-scans can be carried out with dwell times that are typical two orders of magnitude longer compared to conventional EMI receiver technology. Furthermore, the total scan time is reduced for the pre-scan. Final measurements can be performed at the identified frequencies and positions. The short measurement time allows for the measurement of EMI radiation patterns in order to identify EMI sources.

To evaluate the accuracy of the low-noise high-dynamic ultra-broad-band time-domain EMI measurement system the EMI emission of an Intel Celeron 600-MHz has been measured [39]. The measurements have been

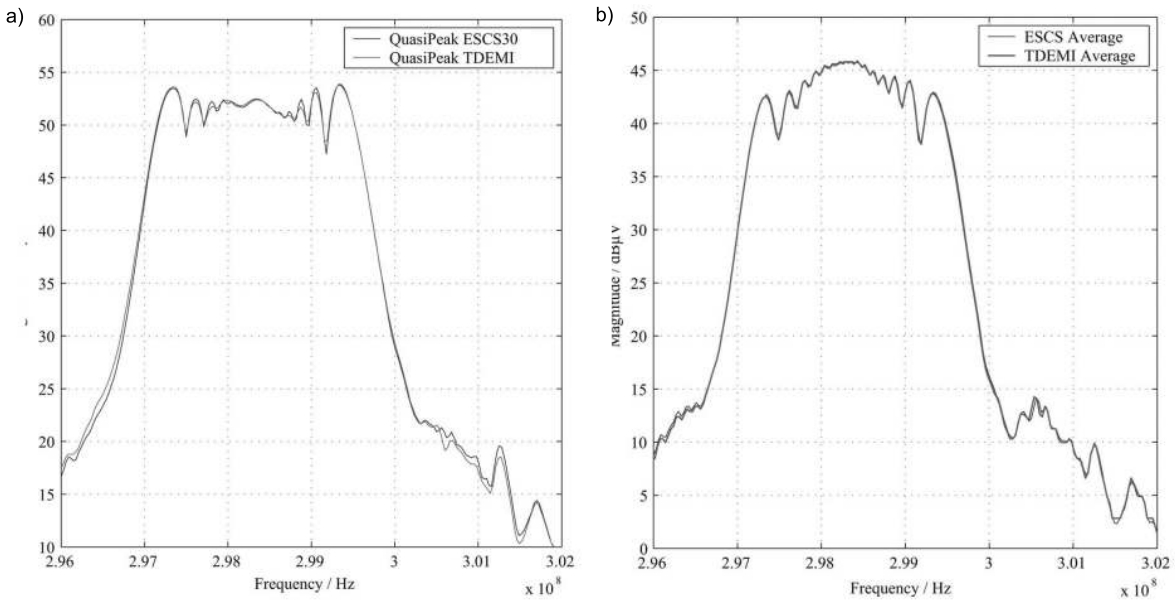

Figure 21: Radiated EMI of desktop computer measured in the frequency interval 296–302 MHz in the (a) quasi-peak detector mode, (b) average mode [39].

compared with measurements performed with a conventional EMI receiver ESCS30 from Rohde & Schwarz.

Figure 20 (a) shows the results of the measurements in the peak detector mode in the frequency interval 296–302 MHz. The dwell time was 100 ms and the frequency step was 30 kHz. The maximum deviation between both measurements is 0.8 dB. Figure 20 (b) shows the radiated EMI measured in the frequency range from 30 MHz to 1 GHz. The dwell time has been 100 ms. The measurement with the time-domain EMI measurement system took 11 s, whereas the measurement with the conventional frequency domain EMI receiver required 50 min. The maximum deviation between both measurements has been 1 dB.

The measurements in the frequency interval 296–302 MHz have also been performed in the quasi-peak detector mode and in the average mode, with frequency steps of 30 kHz in both cases. Figure 21 (a) shows the results of the quasi-peak measurements. The dwell time was 2 s. The maximum difference between the measurements with the time domain EMI measurement system and the results obtained with the EMI receiver have been 0.4 dB. Figure 21 (b) shows the results of the measurements in the average mode. The dwell time has been 4 s. The maximum difference between the measurements with the time domain EMI measurement system and the results obtained with the EMI receiver have been 0.2 dB.

8.3 Time-Domain EMI Measurement Systems for Frequency Bands up to 18 GHz

In order to protect modern electronic systems also above 1 GHz from electromagnetic perturbations and to develop electromagnetic compliant circuits and systems, there is an increasing demand on EMI measurement systems for the frequency bands beyond 1 GHz. Currently such measurements are carried out by using spectrum analyzers and applying the maximum hold function. However, since the traditional EMI receiver can observe only one spectral frequency at the same time and the EMI is changing over a period of seconds, spectrum analyzers are not suited to measure non-stationary EMI with a reasonable scan time. Time-domain EMI measurement systems, using an FFT-based bank of receivers yield short measurement times, and also at frequencies are the better choice beyond 1 GHz.

In [78–81] a broad-band time-domain EMI measurement system for measurements from 9 kHz to 18 GHz

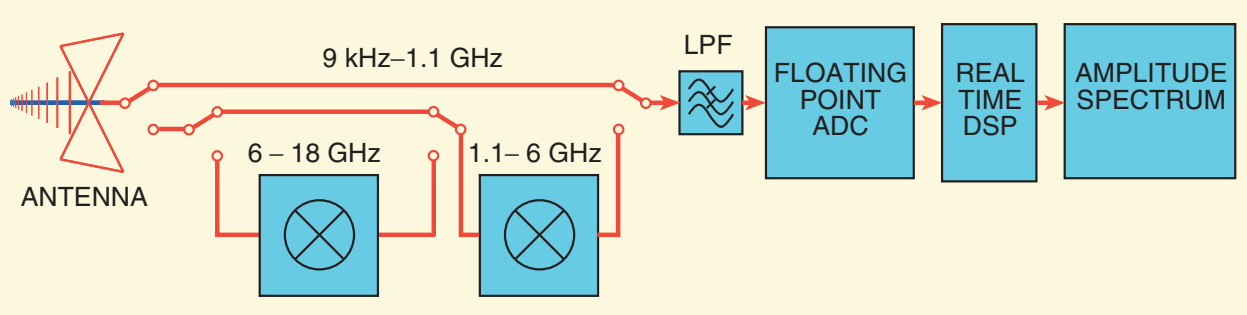

Figure 22: Block diagram of the 9 kHz - 18 GHz time-domain EMI measurement system.

that complies with CISPR 16-1-1 is presented. The combination of floating-point analog-to-digital conversion and digital signal processing on a field-programmable-gate-array (FPGA) with the multi-stage broad-band down-conversion enhances the upper frequency limit to 18 GHz. Measurement times are reduced by several orders of magnitude in comparison to state-of-the-art EMI receivers. The ultra-low system noise floor of 6-8 dB and the spectrogram mode allow for the characterization of the time behavior of EMI near the noise floor.

Figure 22 shows the block diagram of the 9 kHz - 18 GHz time-domain EMI measurement system. For the frequency range from 9 kHz to 1.1 GHz the EMI signal received by the broad-band antenna is directly fed to the 1.1 GHz time-domain EMI measurement system. This 1.1 GHz system corresponds to the system described in the previous section. For frequencies above 1.1 GHz the EMI is down-converted into the base band from 9 kHz to 1.1 GHz. The frequency bands from 1.1 GHz to 6 GHz are down-converted by the down-converter DC1 into the base band. The frequency bands from 6 GHz to18 GHz first are down-converted by the down-converter DC2 into the frequency range from 1.1 GHz to 6 GHz and than further down-converted into the base band.

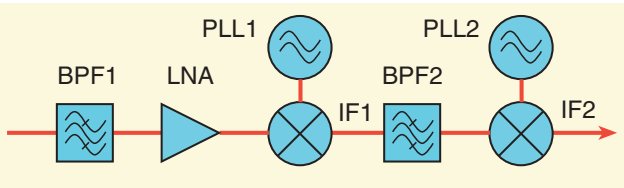

Figure 23: Down-converter for 1.1 GHz - 6 GHz.

Figure 23 shows the block diagram down-converter for the frequecy range from 1.1 GHz to 6 GHz. A two-stage mixing scheme is employed to suppress the image frequency band. The mixer output signal can exhibit the intermediate frequencies [82].

$$f_{IF}^{m,\pm n} = |m f_0 + n f_{rf}| \quad \text{with } m, n \in \mathbb{N}\,, \tag{102}$$

where f_{rf} is the frequency of the RF input signal and f_0 is the local oscillator frequency. The frequency conversion yields two side-bands. The image frequency is converted to the same intermediate frequency band as the input frequency band. The preselection bandpass filter BP1 enhances the spurious -free dynamic range of the system by filtering out high-level out-of band EMI. The RF input band is subdivided into 14 sub-bands with a bandwidth of 325 MHz each. Each of the bands is first up-converted to a high intermediate frequency band IF1, located above the RF input band. This intermediate frequency signal is filtered by a narrow bandpass filter BPF2. By this way the unwanted in-band mixing products are suppressed. A second mixer down-converts the intermediate frequency signal from the IF1 band to the IF2 band which is in the frequency range below 1.1 GHz. PLL1 and PLL2 are the local oscillators, both realized with phase-locked loops.

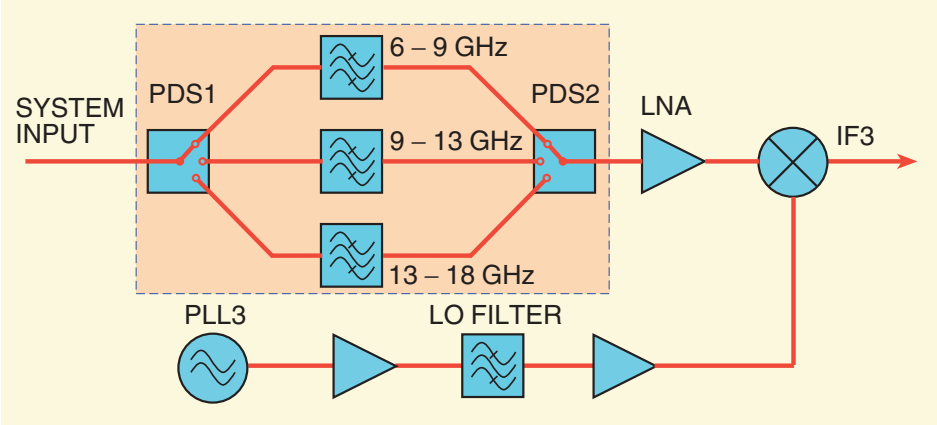

Figure 24: Down-converter for 6 GHz - 18 GHz.

The block diagram of the 6 GHz - 18 GHz down-converter is shown in Fig. 24. The input band is divided into three sub-bands, band 1 from 6 GHz to 9 GHz, band 2 from 9 GHz to 13 GHz, and band 3 from 13 GHz to 18 GHz. The low-insertion-loss single-input - triple-output PIN diode switches PDS1 and PDS2 are used to select the appropriate bandpass filter for the chosen band. These bandpass filters suppress the image bands and the out-of-band interferences. The EMI signal is amplified by a low-noise amplifier and down-converted to the frequency band from 1.1 GHz to 6 GHz via a broad-band mixer with low conversion loss. The local oscillator PLL3 is a low-noise phase locked loop oscillator.

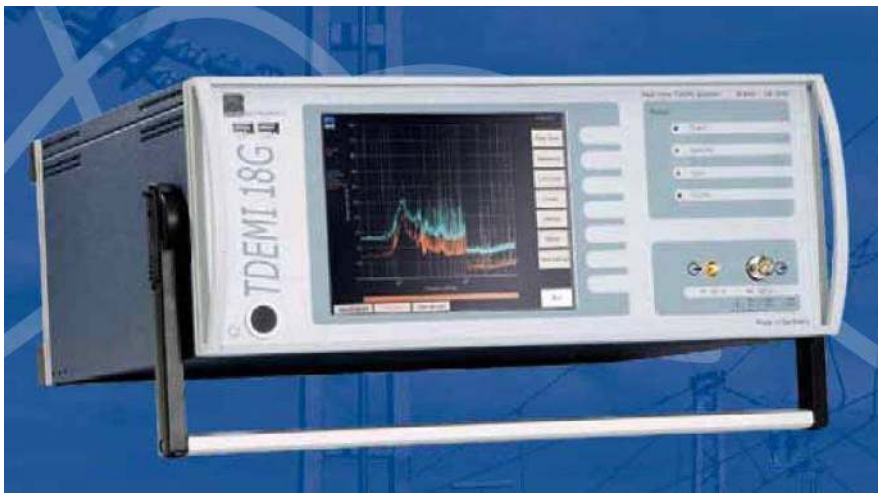

Figure 25: The Gauss Instruments TDEMI 18G® measurement system.

Figure 25 shows a photograph of the Gauss Instruments TDEMI 18G® measurement system for the frequency range from 9 kHz to 18 GHz [77]. This system exhibits the CISPR bandwidths 200 Hz, 9 kHz, 120 kHz, and 1 MHz, and a spurious free dynamic range of about 55 dB. Above 1 GHz it has a significantly lower noise floor than state of the art systems. Emission measurements above 1 GHz are carried out at several angular positions. At each angular position a complete scan is performed. A maximum-hold mode of operation allows to record the maximum values of the spectra. By the report generator the maxima are calculated and listed in a table and the report is generated.

Figure 26 shows the radiated average and quasi-peak EMI spectra of a personal computer with opened cover [79]. The measurements show several narrowband emission lines, supposably originating from the central processing unit, clocked at 2.4 GHz.

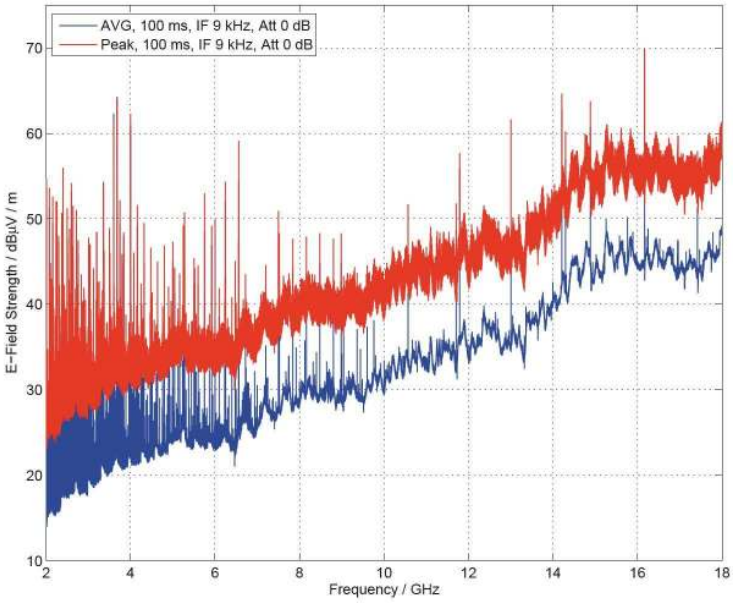

Figure 26: Radiated EMI spectrum of a personal computer [79].

Some household appliances radiate considerable EMI at frequencies beyond 1 GHz. Figure 27 shows the spectrogram of of the radiated emission of the 6^{th} harmonics of a microwave oven [79]. The high sensitivity of the time-domain EMI measurement system facilitates the measurement of the EMI due to the 6^{th} harmonic of the microwave oven magnetron. The measurement of the spectrogram enables the detection of singular and transient events.

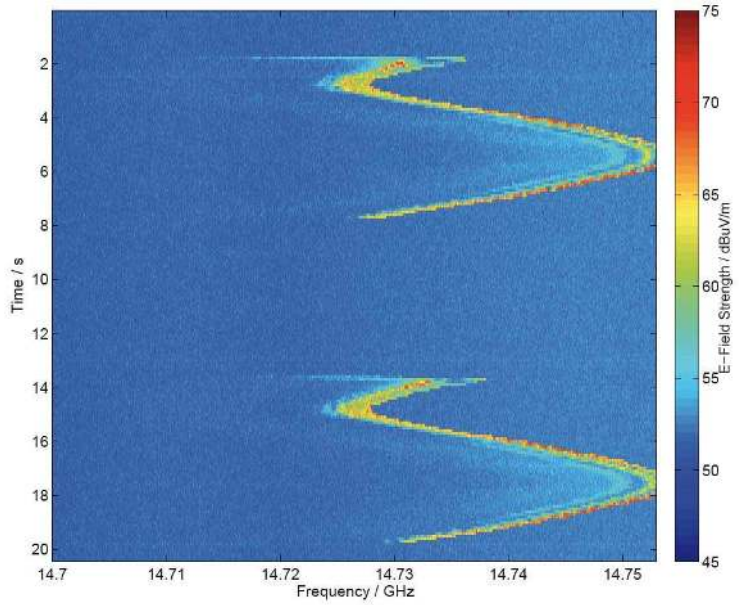

Figure 27: Spectrogram of the radiated emission of the 6^{th} harmonic of a microwave oven [79].

9 Ambient Cancellation Techniques

EMI measurements usually are performed either in shielded anechoic chambers or at open area test sites. Since the inner surfaces of broad-band anechoic chambers must be covered with broad-band radiation absorbent material, anechoic chambers are very expensive, especially if a large size is required. Open area test sites, especially in urban areas, have the disadvantage of unwanted electromagnetic interferers like radio broadcast stations, mobile phone stations and others. An alternative would be to perform the measurement at an open test site in the presence of ambient noise and to use ambient noise cancellation as suggested in [83]. The method described in [83] is based on the use of two coherent EMI receivers fed per two antennas, where one antenna is directed towards the device under test and the other antenna receives the ambient noise. Comparing both received signals the ambient noise can be cancelled. An example of such a system has been presented in [84]. To speed up such measurements the time-domain EMI measurement technique is highly attractive.

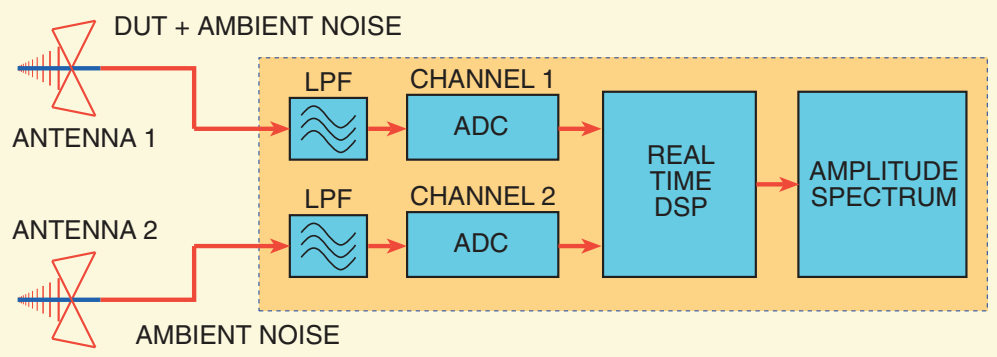

Figure 28: TDEMI measurement system with ambient noise cancellation [40, 41].

An advanced digital signal processing technique for fast measurements of electromagnetic interference in the time-domain at open area test sites has been developed [40, 41].

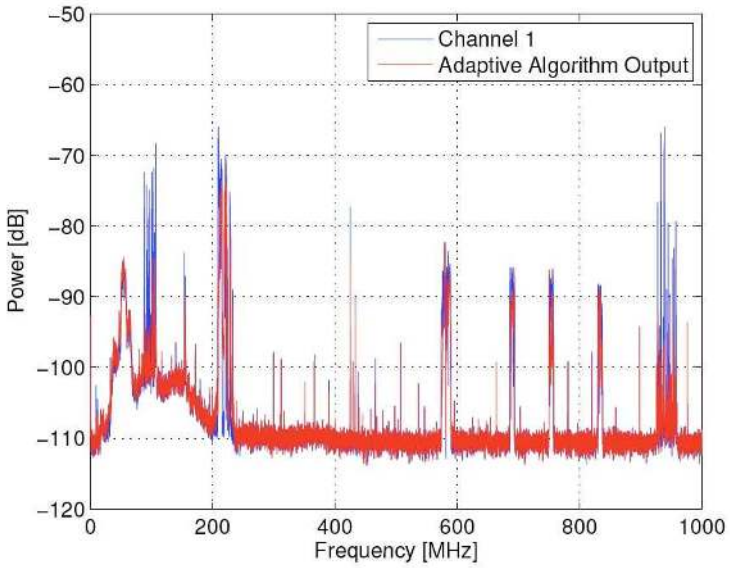

Figure 29: Spectrum of the radiated EMI of a household hand mixer [40].

Measurements performed with this system already have shown the successful cancellation of ambient

noise at an urban test site in the frequency range 30 to 1000 MHz. In this system two channels are used. The two channels are fed from two broad-band antennas, where the first antenna is receiving predominantly the EMI radiated from the device under test and a second antenna receives predominantly the ambient noise. In the two channels both signals are digitized independently and simultaneously.

Figure 29 shows the measured radiated EMI of a household hand mixer as the device under test (DUT). The reference antenna of the measurement setup was separated from the DUT and only received the ambient noise. The EMI measurement system was operated in the average mode and the spectrum was computed with 120 kHz IF bandwidth as required by CISPR 16-1-1 for band C, and D. The algorithm was successful in canceling the ambient noise in the FM band, GSM band, and other frequency components along the spectrum and, hence, the DUT signal was recovered.

10 Conclusions

The foundations of time-domain EMI measurement systems and the realization and performance of time-domain EMI measurement systems were presented in this paper. Examples of commercially available time-domain EMI measurement systems for frequencies up to 18 GHz have been discussed. Modern time-domain EMI measurement systems fulfill the CISPR standards and are suitable for full compliance measurement of EMI. In comparison to a conventional EMI receiver, the measurement time is reduced by a factor up to 4000 for the time-domain EMI measurement system. Depending on the applied IF filter bandwidth, the measurement time is reduced by a factor of 100 for an IF filter bandwidth of 1 MHz, 1000 for an IF filter bandwidth of 120 kHz and by a factor of 4000 for an IF filter bandwidth of 9 kHz.

11 Acknowledgments

This paper is based on research supported by the Deutsche Forschungsgemeinschaft, the Bayerische Forschungsstiftung and the Verein Deutscher Elektrotechniker. The author is indebted to Stephan Braun, Arnd Frech, Christian Hoffmann, Florian Krug, and Hassan H. Slim who have contributed to the development of the systems discussed in this overview. Especially, I want to thank Stephan Braun and Arnd Frech, who together with me founded the GAUSS Instruments GmbH in 2007 for their partnership.

References

[1] C. R. Paul, *Introduction to Elektromagnetic Compatibility.* New York: John Wiley & Sons, 1992.

[2] C. Christopoulos, *Principles and Techniques of Elektromagnetic Compatibility*, ser. ISBN 0-8493–7892–3. CRC Press, 1995.

[3] A. J. Schwab, *Elektromagnetische Verträglichkeit*, ser. ISBN 3-540-60787-0. Springer Verlag, 1996.

[4] "Electromagnetic compatibility," Feb. 2011. [Online]. Available: http://en.wikipedia.org/wiki/Electromagnetic_compatibility

[5] "Directive 2004/108/ec," *Official Journal of the European Union*, vol. L 390, 31Dec. 2004. [Online]. Available: http://ec.europa.eu/enterprise/sectors/electrical/emc/index_en.htm

[6] C. R. Barhydt, "Radio noise meter and its application," *General Electric Rev.*, no. 36, pp. 201–205, 1933.

[7] K. Hagenhaus, "Die Messung von Funkstörungen," *Elektrotechnische Zeitschrift*, vol. 63, no. 15/16, pp. 182–187, April 1942.

[8] E. L. Bronaugh, "An Advanced Electromagnetic Interference Meter for the Twenty-First Century," in *8th International Zurich Symposium On Electromagnetic Compatibility, Zurich, Switzerland, 1989*, 1989, pp. 215–219, no. 42H5.

[9] E. L. Bronaugh and J. D. M. Osburn, "New Ideas in EMC Instrumentation and Measurement," in *10th International Zurich Symposium On Electromagnetic Compatibility, Zurich, Switzerland, 1993*, 1993, pp. 323–326, no. 58J1.

[10] A. Schütte and H. Kärner, "Comparison of time domain and frequency domain electromagnetic compatibility testing," in *Proceedings of the 1994 IEEE International Symposium on Electromagnetic Compatibility*, Aug. 22th–26th, 1994, pp. 64–67.

[11] ——, "Vergleich von EMV-Messungen im Frequenz- und Zeitbereich anhand praktischer Beispiele aus der Fahrzeugtechnik," in *5. Internationale Fachmesse und Kongress für Elektromagnetische Verträglichkeit*, Feb. 20th–22th, 1996, pp. 729–738.

[12] M. Parvis, G. Perrone, and A. Vallan, "A precompliance EMC test-set based on a sampling oscilloscope," *Instrumentation and Measurement, IEEE Transactions on*, vol. 52, no. 4, pp. 1220—1223, 2003.

[13] C. Keller and K. Feser, "Fast emission measurement in time domain," in *14th International Zurich Symposium On Electromagnetic Compatibility, Zurich, Switzerland, 20.–22.2.2001*, 2001, p. 70K7.

[14] ——, "A New Method of Emission Measurement," in *Proceedings of the 2002 IEEE International Symposium on Electromagnetic Compatibility*, 2002, pp. 599–604.

[15] ——, "Improvements in the Fast Emission Measurement in Time Domain," in *2002 International Symposium On Electromagnetic Compatibility Digest, September 9–13, Sorrento, Italy*, 2002, pp. 397–402.

[16] F. Krug and P. Russer, "Ultra-fast broadband EMI measurement in time-domain using FFT and periodogram," in *Proceedings of the 2002 IEEE International Symposium on Electromagnetic Compatibility*, 2002, pp. 577–582.

[17] ——, "Ultra-fast broadband EMI measurement in time domain using classical spectral estimation," in *Microwave Symposium Digest, 2002 IEEE MTT-S International*, vol. 3, 2002, pp. 2237–2240.

[18] ——, "Signal processing methods for time domain EMI measurements," in *Proceedings of the 2003 IEEE International Symposium on Electromagnetic Compatibility*, 2003, pp. 1289–1292.

[19] ——, "A new short-time spectral estimation technique for precompliance measurements," in *ICEAA 2003, International Conference on Electromagnetics in Advanced Applications*, Torino, Italy, September 8th–13th, 2003, pp. 247–250.

[20] ——, "Statistical evaluations of time-domain EMI measurements," in *Proceedings of the 2003 IEEE International Symposium on Electromagnetic Compatibility*, 2003, pp. 1265–1268.

[21] F. Krug, D. Müller, and P. Russer, "Statistical physical noise behavior analysis of the time domain EMI measurement system," in *2003 IEEE AP-S International Symposium on Antennas and Propagation, 22-27.06.2003, Columbus, USA*, 2003, pp. 212–215.

[22] ——, "Signal processing strategies with the TDEMI measurement system," *IEEE Transactions on Instrumentation and Measurement*, vol. 53, no. 5, pp. 1402–1408, 2004.

[23] S. Braun, F. Krug, and P. Russer, "A novel automatic digital quasi-peak detector for a time domain measurement system," in *Proceedings of the 2004 IEEE International Symposium on Electromagnetic Compatibility*, 2004, pp. 919–924.

[24] F. Krug and P. Russer, "Quasi-peak detector model for a time-domain measurement system," *IEEE Transactions on Electromagnetic Compatibility*, vol. 47, no. 2, pp. 320–326, 2005.

[25] S. Braun and P. Russer, "A FPGA based time-domain EMI measurement system for quasi-peak detection and disturbance analysis," in *German Microwave Conference GeMiC 2005, 5–7 April 2005, Ulm, Germany*, 2005, pp. 213–216.

[26] ——, "The dynamic range of a Time-Domain EMI measurement system using several parallel analog to digital converters," in *16th International Zurich Symposium on Electromagnetic Compatibility*, 2005, pp. 203–208.

[27] S. Braun, A. Alt, and P. Russer, "A novel multiresolution high-dynamic ultra-broadband time-domain EMI measurement system," in *2005 International Microwave Symposium Digest, Long Beach, CA, USA*, 2005, p. 4 pp. [Online]. Available: 10.1109/MWSYM.2005.1516918

[28] S. Braun and P. Russer, "A low-noise multiresolution high-dynamic ultra-broad-band time-domain EMI measurement system," *IEEE Transactions on Microwave Theory and Techniques*, vol. 53, no. 11, pp. 3354–3363, 2005.

[29] ——, "Time-domain EMI measurements performed with a multi-resolution system for product development and compliance in," *International Journal of Electromagnetic Compatibility*, pp. 18–26, 2005.

[30] S. Braun, M. Aidam, and P. Russer, "Development of a multiresolution time domain EMI measurement system that fulfills CISPR 16-1," in *Proceedings of the 2005 IEEE International Symposium on Electromagnetic Compatibility*, August 8th–12th, 2005, pp. 388–393.

[31] S. Braun and P. Russer, "Taking time-domain EMI measurements according to international EMC standards," *Compliance Engineering Journal*, vol. XXIII 2006 Annual Reference Guide, no. 1, pp. 45–54, March 2006.

[32] ——, "Measurements of spurious emission with a time-domain EMI measurement system using multi-sampling techniques," in *Proceedings of the 17th International Zurich Symposium on Electromagnetic Compatibility, 2006, EMC Zurich 2006*, vol. 3, Singapore, Feb. 2006, pp. 792–795.

[33] S. Braun, M. Al-Qedra, and P. Russer, "A novel realtime time-domain EMI measurement system based on field programmable gate arrays," in *Proceedings of the 17th International Zurich Symposium on Electromagnetic Compatibility, 2006, EMC Zurich 2006*, Singapore, Feb. 2006, pp. 501–504.

[34] S. Braun, S. Iliev, M. Al-Qedra, and P. Russer, "A real-time multiresolution time-domain EMI measurement system based on ultra-fast high resolution Analog-to-Digital converters," in *Proceedings of the 16th International Conference on Microwaves, Radar & Wireless Communications, MIKON 2006*, 2006, pp. 665–668. [Online]. Available: 10.1109/MIKON.2006.4345268

[35] S. Braun and P. Russer, "Uncertainty analysis and novel test procedures performed with a realtime time-domain EMI measurement system," in *Proceedings of the 2007 IEEE International Symposium on Electromagnetic Compatibility*, 2007, pp. 1–4.

[36] ——, "An emission measurement system for the twenty-first century based on time-domain measuring methods," *The International Journal of Electromagnetic Compatibility*, vol. Interference Technology, Directory & Design Guide 2007, Feb. 2007.

[37] S. Braun, M. Aidam, and P. Russer, "Development and evaluation of a realtime Time-Domain EMI measurement system for automotive testing," in *Proceedings of the 2007 IEEE International Symposium on Electromagnetic Compatibility*, Honolulu, HI, USA, July 9th–13th, 2007, pp. 1–4.

[38] S. Braun, A. Frech, and P. Russer, "A low-noise realtime time-domain EMI measurement system," in *Electromagnetic Compatibility, 2007. EMC Zurich 2007. 18th International Zurich Symposium on*, 2007, pp. 381–384.

[39] S. Braun, T. Donauer, and P. Russer, "A real-time time-domain EMI measurement system for full-compliance measurements according to CISPR 16-1-1," *IEEE Transactions on Electromagnetic Compatibility*, vol. 50, no. 2, pp. 259–267, 2008.

[40] A. Frech, A. Zakaria, S. Braun, and P. Russer, "Ambient noise cancelation with a time-domain EMI measurement system using adaptive filtering," in *Proceedings of the Asia-Pacific Symposium on Electromagnetic Compatibility and 19th International Zurich Symposium on Electromagnetic Compatibility, 2008. APEMC 2008*, 2008, pp. 534–537.

[41] A. Frech, S. Braun, and P. Russer, "Time-domain EMI measurements in the presence of ambient noise," in *Proceedings of the 2008 IEEE International Symposium on Electromagnetic Compatibility*, 2009, pp. 139–142.

[42] CISPR16-1, *Specification for radio disturbance and immunity measuring apparatus and methods Part 1: Radio disturbance and immunity measuring apparatus*, 2nd ed. International Electrotechnical Commission, 2007.

[43] CISPR16-2, *Specification for radio disturbance and immunity measuring apparatus and methods Part 2: Methods of measurement of disturbances and immunity.* International Electrotechnical Commission, 1999.

[44] CISPR16-1-1, Ed. 3.1 Am. 1, *Specification for radio disturbance and immunity measuring apparatus and methods Part 1-1: Radio disturbance and immunity measuring apparatus – Measuring apparatus.* International Electrotechnical Commission, 2010.

[45] "IEC – International Electrotechnical Commission – standards developed," Feb. 2011. [Online]. Available: http://www.iec.ch/standardsdev/

[46] "Comité International Spécial des Perturbations Radioélectriques," Feb. 2011. [Online]. Available: http://en.wikipedia.org/wiki/Comit%C3%A9_International_Sp%C3%A9cial_des_Perturbations_Radio%C3%A9lectriques

[47] International Organization for Standardization, "International Standards for Business, Government and Society," Feb. 2011. [Online]. Available: http://www.iso.org/iso/home.html

[48] European Committee for Electrotechnical Standardisation, Feb. 2011. [Online]. Available: http://www.iso.org/iso/home.html

[49] European Telecommunications Standards Institute, Feb. 2011. [Online]. Available: http://www.iso.org/iso/home.html

[50] Federal Communications Commission, Feb. 2011. [Online]. Available: http://en.wikipedia.org/wiki/Federal_Communications_Commission

[51] "American national standard for electromagnetic noise and field strength instrumentation, 10 hz to 40 GHz specifications," 2009.

[52] S. Braun, "Theorie und Anwendung von Zeitbereichsverfahren zur nonkonformen EMV-Emissionsmessung," Dissertation, Technische Universität München, München, 2007.

[53] A. Bowman and A. W. Azzalini, *Applied Smoothing Techniques for Data Analysis.* Oxford University Press, 1997.

[54] S. Linkwitz, "Measurement of narrowband and broadband emissions using peak and average detection," in *1987 IEEE International Symposium On Electromagnetic Compatibility Digest*, Aug. 25–27 1987, pp. 36–41.

[55] R. L. Belding, "Receiver measurements near the noise floor," in *IEEE International Symposium On Electromagnetic Compatibility Digest*, San Diego, Sep. 16–18 1986, pp. 24–31.

[56] C. F. Gauss, "Theoria interpolationis methodo nova tractata," in *Gauss' collected works.* Göttingen, Germany: Goettingen State and University Library, 1886, pp. 265–330.

[57] J. B. J. Fourier, *Théorie analytique de la chaleur.* Firmin Didot, 1822.

[58] P. G. L. Dirichlet, "Sur la convergence des séries trigonométriques qui servent à représenter une fonction arbitraire entre des limites données," *Journal für die reine und angewandte Mathematik*, vol. 4, pp. 157–169, 1829.

[59] R. Bracewell, *Fourier Transform and its Applications.* New York: McGraw-Hill, 1999.

[60] A. V. Oppenheim and R. W. Schafer, *Discrete-Time Signal Processing*, 2nd ed., ser. Signal Processing Series. (Prentice-Hall, 1989.

[61] R. L. Allen and D. W. Mills, *Signal Analysis.* IEEE Press, John Wiley & Sons, 2004.

[62] W. B. Davenport and W. L. Root, *An Introduction to the Theory of Random Signals and Noise.* Wiley-IEEE Press, Oct. 1987.

[63] D. Middleton, *An Introduction to Statistical Communication Theory: An IEEE Press Classic Reissue*, 1st ed. Wiley-IEEE Press, Apr. 1996.

[64] P. Russer and S. Müller, "Noise analysis of linear microwave circuits," *International Journal of Numerical Modelling, Electronic Networks, Devices and Fields*, vol. 3, pp. 287–316, 1990.

[65] P. Russer, "Noise analysis of linear microwave circuits with general topology," *The review of radio science 1993–1996, Oxford, England,*, pp. 887–890, 1996.

[66] S. L. Marple, *Digital Spectral Analysis*. Prentice Hall, Jan. 1987.

[67] E. O. Brigham, *Fast Fourier Transform, The*. Prentice-Hall, 1974.

[68] M. Mandal and A. Asif, *Continuous and Discrete Time Signals and Systems*, 1st ed. Cambridge University Press, Sep. 2007.

[69] P. S. R. Diniz, E. A. B. da Silva, and S. L. Netto, *Digital Signal Processing: System Analysis and Design*, 2nd ed. Cambridge University Press, Sep. 2010.

[70] J. W. Cooley and J. W. Tukey, "An algorithm for the machine calculation of complex fourier series," *Mathematics of computation*, vol. 19, no. 90, pp. 297–301, 1965.

[71] M. H. Hayes, *Statistical Digital Signal Processing and Modelling*. New York: John Wiley & Sons, Inc., 1996.

[72] M. S. Bartlett, "Smoothing periodograms from time series with continous spectra," *Nature*, vol. 161, no. 686–687, 1948.

[73] P. Welch, "The use of fast fourier transform for the estimation of power spectra: A method based on time averaging over short, modified periodograms," *Audio and Electroacoustics, IEEE Transactions on*, vol. 15, no. 2, pp. 70 – 73, Jun. 1967.

[74] F. Krug and P. Russer, "The time-domain electromagnetic interference measurement system," *Electromagnetic Compatibility, IEEE Transactions on*, vol. 45, no. 2, pp. 330–338, 2003.

[75] H. So, Y. Chan, Q. Ma, and P. Ching, "Comparison of various periodograms for sinusoid detection and frequency estimation," *Aerospace and Electronic Systems, IEEE Transactions on*, vol. 35, no. 3, pp. 945 –952, Jul. 1999.

[76] S. Braun, C. Hoffmann, A. Frech, and P. Russer, "A realtime time-domain EMI measurement system for measurements above 1 GHz," in *Electromagnetic Compatibility, 2009. EMC 2009. IEEE International Symposium on*, 2009, pp. 143–146.

[77] "GAUSS Instruments high speed measurements." [Online]. Available: http://www.gauss-instruments.com/

[78] C. Hoffmann, S. Braun, and P. Russer, "A broadband time-domain EMI measurement system for measurements up to 18 GHz," in *Proceedings of the European Conference on Electromagnetic Compatibility, 2010, EMC Europe 2010*, Wroclaw, Poland, September 13th - 17th, 2010, pp. 1–4.

[79] C. Hoffmann and P. Russer, "A time-domain system for CISPR 16-1-1 compliant measurements above 1 GHz," in *Proceedings of the Asia-Pacific Symposium on Electromagnetic Compatibility, Jeju Island, Korea May, 16–19, 2011. APEMC 2011*, 2011, pp. 1–4.

[80] ——, "A time-domain system for emi measurements above 1 ghz with high sensitivity," in *German Microwave Conference GeMiC 2011, 14–16 March 2011, Darmstadt, Germany*, 2011, pp. 1–4.

[81] ——, "A real-time low-noise ultra-broadband time-domain EMI measurement system up to 18 GHz," *to be published in IEEE Transactions on Electromagnetic Compatibility*, pp. 1–8, 2011.

[82] S. A. Maas, *Microwave Mixers*. Boston: Artech House, 1993.

[83] T. Shinozuka and A. Sugiura, "Reduction of ambient noise in emi measurement," in *IEEE International Symposium On Electromagnetic Compatibility Digest*, Nagoya, Japan, September 8-10 1989, pp. 24–28.

[84] P. Parhami, M. Marino, S. Watkins, and E. Nakauchi, "Innovative precompliance test methodology using ambient cancellation and coherence detection techniques," in *IEEE International Symposium On Electromagnetic Compatibility*, Seattle, USA, Aug. 2-6 1999, pp. 1022–1025.